



AMERICAN UNIVERSITY OF BEIRUT

EXPERIMENTAL ASSESSMENT OF  
EXTERNAL AND INTERNAL GEOGRID  
CONFINEMENT OF REINFORCED  
CONCRETE COLUMNS

by  
RUBA HASAN BASHIR

A thesis  
submitted in partial fulfillment of the requirements  
for the degree of Master of Engineering  
to the Department of Civil and Environmental Engineering  
of Maroun Semaan Faculty of Engineering and Architecture  
at the American University of Beirut

Beirut, Lebanon  
May 2021

AMERICAN UNIVERSITY OF BEIRUT

EXPERIMENTAL ASSESSMENT OF  
EXTERNAL AND INTERNAL GEOGRID  
CONFINEMENT OF REINFORCED  
CONCRETE COLUMNS

by  
RUBA HASAN BASHIR

Approved by:

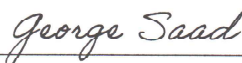
\_\_\_\_\_  
Dr. Bilal Hamad, Professor  
Civil and Environmental Engineering

\_\_\_\_\_  
Advisor


\_\_\_\_\_  
Dr. Ghassan Chehab, Associate Professor  
Civil and Environmental Engineering

\_\_\_\_\_  
Member of Committee



\_\_\_\_\_  
Dr. George Saad, Associate Professor  
Civil and Environmental Engineering

\_\_\_\_\_  
Member of Committee

Date of thesis defense: May 4, 2021



# Acknowledgements

I would like to thank all who contributed to the completion of this thesis no matter how small the contribution was. First and foremost, I give thanks to Allah for giving me the knowledge and strength to complete this work.

I would like to express my sincere gratitude to my thesis advisor Professor Bilal Hamad for his invaluable advice, continuous support, and patience throughout my master's degree. His immense knowledge and plentiful experience have inspired me in both my academic research and daily life.

I would also like to thank Professor George Saad for his technical support, especially for his help in the analytical aspects, and for Professor Ghassan Chehab for participating in my thesis committee and for his insightful comments and suggestions.

Moreover, I am deeply grateful to Mr. Helmi El-Khatib, Manager of the Civil and Environmental Engineering labs, for his never-ending help and support. Also, I would like to express my sincere gratitude to Ms. Dima Al-Hassanieh, CEE Lab Assistant manager, for her assistance at every stage of the research project. Her teachings and guidance has certainly made the lab experience more enjoyable.

I cannot forget to extend my sincere thanks to the CEE lab staff members Mr. Abdel Rahman Sheikh and Bashir Asyala for using their experience to guide me in the experimental phase.

In addition, I would like to thank my friends for their continuous support, encouragement, and help throughout the past three years, I could not have done this without you all. In particular, I would like to offer my special thanks to my engineering friends and colleges, Ms. Arij Hawari, Mr. Loai Al-Mawed, and Mr. Mahmoud Khadija for their valuable assistance throughout all the master's phases.

I am forever thankful for my mom who has worked so hard to get me where I am today and to my siblings who always show unparalleled love, help, and support whenever I call on them.

Finally, I would love to dedicate this thesis to my late father. Thank you for inspiring me in every stage of my life.

# An Abstract of the Thesis of

Ruba Hasan Bashir for Master of Engineering  
Major: Civil Engineering

Title: Experimental Assessment of External and Internal  
Geogrid Confinement of Reinforced Concrete Columns

The use of fiber-reinforced polymer (FRP) as an external column confinement and retrofitting material has been dominant. However, researchers have been experimenting other methods due to the FRP high cost. Recent research has shown the efficacy of Geogrid as a geo-synthetic material as an internal reinforced concrete column confinement. This study investigates experimentally the feasibility of using geogrid material as an external column confinement as compared to FRP and flexible bitumen coated E-glass textile. The test variables are transverse reinforcement spacing, confinement material (Geogrid, Bitumen coated E-glass textile, or FRP), type of geogrid (uniaxial or biaxial), number of confinement layers (one or two), and confinement location (internal or external). A total of 39 small-scale column specimens were tested under uniaxial compression. Assessment of the variable was done by analyzing the axial load-displacement behavior, the modes of failure, and the structural ductility measured by fracture energy and energy dissipation. Results show that the external confinement of reinforced concrete columns using geogrid can significantly enhance the strength, ductility, and energy capacity of the specimen. An analytical confinement model to predict the ultimate stress of the specimen using geogrid and bitumen textile was developed from existing confinement model for FRP. Comparison between the confinement stress model and the experimental results provided satisfactory predictions for the ultimate stress. This study provided promising results for the use of geogrid as an external confinement for reinforced concrete columns despite the fact that the tensile strength of the geogrid is significantly lower than that of synthetic FRP.

Keywords: Geogrid; uniaxial geogrid; biaxial geogrid; bitumen coated E-glass textile; stirrups; transverse reinforcement; fiber reinforced polymer (FRP); ex-

ternal confinement; concrete; columns; confined concrete; ductility enhancement;  
confinement model

# Contents

<b>Acknowledgements</b>	<b>v</b>
<b>Abstract</b>	<b>vi</b>
<b>1 Introduction</b>	<b>1</b>
1.1 Research objectives . . . . .	2
1.2 Problem statement . . . . .	2
1.3 Thesis organization . . . . .	3
<b>2 Background and Literature Review</b>	<b>4</b>
2.1 Geogrid: definition, usage, classification and advantages . . . . .	5
2.2 Internal confinement . . . . .	6
2.3 External confinement . . . . .	7
2.3.1 Action of FRP confinement . . . . .	7
2.3.2 FRP stress-strain curves type . . . . .	8
2.3.3 Reinforced concrete external confinement . . . . .	10
2.3.4 Fracture mechanics . . . . .	12
2.3.5 ACI recommendations . . . . .	13
<b>3 Experimental Program</b>	<b>16</b>
3.1 Pilot test . . . . .	16
3.1.1 Geogrid tensile test . . . . .	17
3.1.2 Concrete . . . . .	18
3.1.3 Epoxy . . . . .	19
3.1.4 Testing . . . . .	19
3.1.5 Test results . . . . .	19
3.2 Research full experimental program . . . . .	20
3.2.1 Test Specimens and Test Parameters . . . . .	20
3.2.2 Material and specimens preparation . . . . .	21
<b>4 Test Results and Analysis</b>	<b>32</b>
4.1 Mode of failure . . . . .	32
4.1.1 Specimens internally confined with ties . . . . .	32



4.1.2	Specimens internally confined with uniaxial or biaxial geogrids . . . . .	33
4.1.3	Specimens with external confinement . . . . .	34
4.2	Test result and analysis . . . . .	37
4.2.1	Effect of the stirrups spacing . . . . .	41
4.2.2	Effect of confinement type . . . . .	41
4.3	Prediction of ultimate axial stresses . . . . .	47
<b>5</b>	<b>Conclusion and Recommendations</b>	<b>50</b>
5.1	Conclusion . . . . .	50
5.2	Recommendation . . . . .	51
<b>A</b>	<b>Biaxial Geogrid Confinement Model Example</b>	<b>52</b>

# List of Figures

2.1	Confining action of FRP jacket . . . . .	8
2.2	Classification of stress–strain curves of FRP-confined concrete. (a) Increasing type; (b) Decreasing type with $f'_{cu} \geq f'_{co}$ ; (c) Decreasing type with $f'_{cu} < f'_{co}$ . [Lam and Teng, 2003] . . . . .	9
2.3	Column Failure Modes . . . . .	13
2.4	Lam and Teng’s stress-strain model for FRP-confined concrete [Lam and Teng, 2003] . . . . .	14
3.1	Stress-strain curve for the biaxial geogrid [Daou, 2018] . . . . .	17
3.2	Biaxial Geogrid . . . . .	18
3.3	Pilot test cast specimens . . . . .	18
3.4	Pilot test specimens after testing . . . . .	20
3.5	View of all cast specimens . . . . .	22
3.6	Biaxial Geogrid . . . . .	24
3.7	Uniaxial Geogrid . . . . .	24
3.8	Bitumen coated E-glass textile . . . . .	24
3.9	Tensile testing of the geogrid and bitumen textile sheets . . . . .	25
3.10	Tensile testing stress-strain curve for biaxial and uniaxial geogrid . . . . .	25
3.11	Schematics of the test specimens . . . . .	29
3.12	Specimens preparation . . . . .	30
3.13	LVDT’s mounting frame . . . . .	30
3.14	Schematic diagram of the test setup . . . . .	31
3.15	Actual view of the testing machine . . . . .	31
4.1	Failure of specimens with different transverse tie spacing . . . . .	33
4.2	Failure modes of the specimens internally confined using biaxial and uniaxial geogrid . . . . .	34
4.3	Failure modes of specimens externally confined using biaxial and uniaxial geogrid . . . . .	35
4.4	Failure modes of the specimens externally confined using bitumen textile sheets . . . . .	36
4.5	Failure modes of specimens externally confined using FRP sheets . . . . .	37
4.6	Schematic load-displacement curve to define the parameters used in Table 4.1 . . . . .	39

4.7	Ratio of ultimate axial load capacity values of all tested specimens relative to S20 . . . . .	39
4.8	Average displacement ductility index values of all tested specimens	40
4.9	Average energy ductility index values of all tested specimens . . .	40
4.10	Load-displacement curves for specimens with different stirrup spacing . . . . .	41
4.11	Load-displacement curves for internally confined specimens . . . .	43
4.12	Load-displacement curves of geogrid and bitumen textile externally confined specimens along with specimens S20 (Control) and S10 . . . . .	44
4.13	Load-displacement curves of internally and externally confined biaxial geogrid Specimen, single and double layered . . . . .	45
4.14	Load-displacement curves of internally and externally confined biaxial geogrid Specimen, single and double layered . . . . .	45
4.15	Load-displacement curves of geogrid and FRP Sheet externally confined specimens . . . . .	46

# List of Tables

3.1	Pilot test variables . . . . .	16
3.2	Physical and mechanical properties of the Biaxial Geogrid . . . . .	17
3.3	Epoxy Properties . . . . .	19
3.4	Test variables . . . . .	21
3.5	Batching weights per cubic meter of concrete for the two concrete mixes used . . . . .	22
3.6	Physical and mechanical properties of the Biaxial Geogrid . . . . .	23
3.7	Physical and mechanical properties of the Uniaxial Geogrid . . . . .	23
3.8	Mechanical properties of the bitumen coated E-glass textile [Hara- jli et al., 2010] . . . . .	24
3.9	Properties of the CFRP SikaWrap - 230 C . . . . .	26
3.10	Mechanical characteristics of the steel bars . . . . .	26
4.1	Test Results . . . . .	38
4.2	Results of the analytical model without reduction factor . . . . .	49
4.3	Results of the analytical model applying a reduction factor . . . . .	49

# Chapter 1

## Introduction

Columns are critical reinforced concrete members whose failure potentially leads to structural collapse. In regions where earthquakes occur, reinforced concrete columns with insufficient transverse reinforcement have historically behaved in a brittle manner resulting in structural failures that led to financial losses as well as human fatalities. In the aftermath of earthquake activities, strengthening and rehabilitation procedures have been employed to increase the structural capacity and ductility of under-designed cracked columns. The procedures include jacketing the existing columns with structural steel plates or high performance reinforced concrete jackets. In the last few decades, research conducted on the external confinement of columns with fiber-reinforced polymer (FRP) sheets has shown a positive impact on the ultimate strength, axial stress-strain capacity, and ductility ([Pessiki et al., 2001] and [Ilki et al., 2008]).

Fiber-reinforced polymer (also called fiber-reinforced plastic) is a composite material made of a polymer matrix reinforced with fibers such as carbon and glass. FRP has been used extensively as a retrofitting material in the construction industry due to the following advantageous properties: high level of stiffness, lightweight, good electrical insulating properties, high strength to weight ratio, ease of handling and fabrication, and corrosion resistance. The research reported in the literature validates that FRP enhances both the compressive strength and the axial strain corresponding to peak axial stresses [Parvin and Wang, 2001].

On the other hand, the dominance of FRP as a retrofitting material did not diminish the drive to find an equivalent or better-performing material to compete with FRP in the construction industry. In the 1950s, a material called geogrid, which is a geosynthetic polymer, was found to strengthen the soil by mobilizing high soil-reinforcement bond stress, providing high tensile stiffness, and enhancing load-settlement characteristics. Geogrids are strong in tension allowing them to transfer forces to a larger area of soil [Hernandez et al., 2015]. Later, a new type of geogrid was fabricated that showed good performance in pavement applications. It performed the two major strengthening functions: separation and reinforcement [Das, 2016]. Numerous research projects that were performed on

the use of geogrid for soil and pavement applications, proved that geogrids are a practical and economical strengthening material in these domains. Lately, significant concerns have been raised about the effectiveness of geogrids in concrete applications leading to a research program being conducted on the use of geogrid sheets as a replacement for conventional longitudinal and transverse reinforcing steel bars [Daou, 2018] and [Daou et al., 2020]. Recently, geogrid sheets were found to improve both the compressive strength and ductility of circular concrete columns when used as an internal confining material [Daou, 2018] and [Daou et al., 2020]. The research reported in this thesis investigates the effect of using geogrids to externally confine circular concrete columns in comparison with FRP external confinement and internal geogrid confinement. In the experimental work presented here, the columns are subjected to a concentric monotonic axial compression force. In addition to the experimental program and analytical models are developed.

## 1.1 Research objectives

The main objective of the research program described in this proposal is to evaluate experimentally the axial load capacity and load-displacement response of small-scale reinforced concrete columns. The columns are either internally or externally confined with stiff uniaxial and biaxial geogrids and flexible bitumen textile. Assessment of the effectiveness of geogrids confinement shall be conducted by comparing different modes of internal confinement (transverse reinforcement and geogrids) and external confinement (FRP, geogrids, and bitumen textile). Comparison is based on load capacity, mode of failure, load-displacement history, and energy absorption.

## 1.2 Problem statement

Recently, there has been increasing use of geogrids to strengthen soils and pavements. There are significant practical applications. The hypothesis, that such strengthening procedure could be extended to providing effective external confinement, has significant practical applications. The novelty of this research stems from the fact that there is currently no published research on using geogrids as an alternative external confinement procedure for columns. The proposed research provides a better understanding of the axial load-displacement response of internally or externally confined reinforced concrete circular columns using geogrids. Experimental investigation of different confinement modes will be analyzed, and analytical models will be developed to predict the structural response. It would be significant to check if the external confinement of reinforced concrete columns with geogrids would be effective as the proven FRP confinement.

The research program consists of experimental and analytical investigations, and its scope includes the following:

1. Review of previous research on the use of geogrids in concrete structures and the use of FRP to externally confine columns.
2. Design and assembly of an experimental set-up suitable for testing small-scale columns under constant axial compression and incrementally increasing lateral deformation.
3. Design, construction, and instrumentation of fifteen full-scale circular columns with conventional longitudinal reinforcement and geogrid sheets as an internal transverse reinforcement or external confining material.
4. Testing of thirty-seven columns under combined axial compression while recording the relevant test data by means of data acquisition systems.
5. Evaluation of test data and investigation of the effects of test parameters including the spacing of the internal transverse reinforcement or ties, type of geogrid (uniaxial, biaxial or flexible biaxial), number of geogrid layers (one or two), location of geogrid (internal or external), and FRP external jacketing.
6. Development of numerical models for stress-strain relationships for concrete with geogrids sheets.
7. Preparation of thesis and presentation of results.

### **1.3 Thesis organization**

This thesis is organized into five chapters. Chapter 1 is an introduction to the research topic and the hypothesis it intends to address. Chapter 2 provides background information about geogrids followed by a literature review on the use of geogrids in concrete pavement, beams, and columns, in addition to the use of FRP as a confining material for beams and columns. Chapter 3 explores in detail: the experimental program, test variables, and materials used in the research. Chapters 4 includes a full description and analysis of the test results providing data on the general behavior and mode of failure, the effect of geogrids application internally and externally, and the axial stress versus lateral strain representation of the specimens. Finally, Chapter 5 summarizes the major conclusions and provides recommendations for further research.

## Chapter 2

# Background and Literature Review

Ductility relates the ability of the structure to deform significantly before reaching failure or collapse; this is a crucial criterion in earthquake engineering. Ductility in concrete is defined by the percentage of steel reinforcement as concrete does not contribute to ductility. Mild steel is an example of a ductile material that can be bent and twisted without rupture. Before 1975, the U.S. building codes and construction standards did not consider ductility as a design parameter [Fajfar, 2018]. Subsequently, most of the buildings constructed before 1975 are believed to be non-ductile, stiff buildings which cannot resist the large seismic deformations. That explains the brittle failure of buildings in regions subjected to earthquakes as seen during the 1971 San Fernando earthquake.

After 1975, a ductility requirement was established in the seismic design codes and construction standards in high seismic risk areas [Fajfar, 2018]. Numerous studies were conducted on the improvement of ductility of structures during the design stage and on the ductility of already existing structures. For the design stage, several techniques were investigated to increase the ductility of a structure with minimum steel reinforcement due to economic purposes. The following materials were tested and proved effective: steel fibers [Kal et al., 2009], synthetic fibers [Mirmiran et al., 1998], geogrid ([Daou, 2018] and [Daou et al., 2020]), etc. However, larger concerns have been raised to increase the capacity and the ductility of the under-designed and already existing structures. Several techniques were investigated in this domain including steel jacketing to FRP [Wu et al., 2006], which was considered a revolution in the construction maintenance industry. Also, codes and standards were developed and modified as in the case of the ACI Building Code ACI 318-11 which changed the requirements for steel confinement in the most critical sections of concrete columns and walls.

One of the major disadvantages of the current retrofitting techniques such as steel plate or FRP or external jacketing is the high cost. This economical issue increased the drive to find a more economical solution making geogrid, a geosyn-



thetic material, a possible replacement for FRP, knowing that geogrid showed effectiveness in soil [Hernandez et al., 2015], pavement tensile strengthening [Das, 2016], and promising results in concrete application ([Daou, 2018]; [Das et al., 2010]; [El Meski and Chehab, 2014]; [Itani et al., 2016]).

In this chapter, the literature review appraises four major items necessary for this study. The first part is a general view of the geogrid as a material, its types and classifications, its use throughout history, and its considerable advantages. The second part summarizes information from previous studies on the internal confinement of reinforced concrete columns. The third part elaborates on the existing research regarding the retrofitting techniques for existing columns using several materials as external confinement.

## **2.1 Geogrid: definition, usage, classification and advantages**

Geogrid is a geosynthetic material consisting of connected parallel sets of tensile ribs with apertures of sufficient size to allow strike-through of the surrounding soil, stone, or other geotechnical material [Ghafoori et al., 2016]. They are made from polymers such as polypropylene, polyethylene, or polyester. They are commonly used for soil stability purposes in road embankments [Maxwell, 2005] and reinforced earth walls due to their tensile reinforcing capability [Palmeira et al., 2008].

Types of geogrids, currently available in the market, include welded geogrid, extruded geogrid, and woven geogrid [Das et al., 2010]. Uniaxial, biaxial, and triaxial geogrids are the extruded geogrid classifications based on the reinforcement direction [El Meski and Chehab, 2014]. Geogrids which are pre-tensioned in one direction are called uniaxial geogrids. This type is used mainly in geotechnical applications such as retaining walls, reinforcing slopes, and embankments. Geogrids pre-tensioned in two directions are called biaxial geogrids, used in pavement applications when the principal stress direction is uncertain such as unpaved roads, flexible pavement and railroads [Das et al., 2010]. When subjected to tension in more than two directions, biaxial geogrids cannot provide constant tensile strength leading to a new geogrid classification: triaxial geogrids. Triaxial geogrids provide uniform tensile strengths in all directions compared with uniaxial and biaxial geogrids, yet their effects on the performance of reinforced pavements have not been well-tested and evaluated [El Meski and Chehab, 2014].

Geogrids are known for their high tensile strength which adds shear strength at the interface between the surrounding material and the geogrid [Tang et al., 2008], as well as their excellent chemical resistance given that they are made from polymers [Das, 2016]. These two properties led researchers to start considering geogrids as an alternative to steel reinforcement in concrete [Tang et al., 2008].

## 2.2 Internal confinement

[Chidambaram and Agarwal, 2014] investigated the effect of geogrids in confining conventional concrete and steel fiber reinforced concrete (SFRC) under compression and split tension. Four types of 150x300 mm cylindrical specimens were tested: conventional, SFRC, internal geogrid confinement (GC), and GC with SFRC. The experimental results indicated that internal geogrid confinement improved the axial stress-strain behavior of specimens loaded in compression as compared to conventional concrete specimens. The improvement was more significant when using SFRC. Geogrids and steel fibers changed the failure mechanism of the specimens from sudden brittle behavior to ductile without significant loss of strength. As for the specimens tested in split tension, geogrid confinement did not increase the tensile strength but helped the specimens sustain larger displacements.

[Al-Ayash et al., 2015] conducted an experimental study to assess the advantages of using geogrids as a confinement tool in plain cement concrete (PCC) cylinders taking into consideration different types of geogrids (uniaxial and biaxial) and a different number of reinforcement layers (one layer and two layers). The tensile strength of the biaxial geogrids was lower than that of the uniaxial ones in the study. Cylinders confined with two layers of uniaxial geogrid hoops showed the highest ductility after the initial cracking of concrete. Cylinders confined with two layers of biaxial geogrids were not tested. Cylinders confined with one layer of uniaxial geogrid or one layer of biaxial geogrid showed similar behavior in the post-cracking phase to cylinders confined with steel hoops. In addition, the cylinder confined with one layer of biaxial geogrid had the highest ultimate axial load. This indicates that the mesh shape of the biaxial geogrid is what resulted in additional compressive strength (due to better confinement effect) rather than the geogrid's tensile strength since the tensile strength of biaxial geogrids was lower than that of the uniaxial type.

[Sivakamasundari et al., 2017] investigated the effectiveness of using biaxial geogrids as shear reinforcement along with steel fibers. The compressive and tensile behavior of three types of specimens were compared: a control cylinder made of plain concrete, another one confined with a tubular-shaped biaxial geogrid, and a third one like the second but adding steel fibers. Test results showed that the use of geogrid confinement with steel fiber reinforced concrete (SRFC) increased both the compressive and tensile strength of the cylindrical specimens. In another experiment, concrete beams with different shear reinforcement techniques were cast and tested under three-point monotonic loading: a control beam transversally reinforced with steel stirrups only, another beam containing steel stirrups and biaxial geogrid-transverse reinforcement in the plastic hinge region, and a third one with SFRC along with steel stirrups and geogrids. It was concluded that the use of geogrids and transverse reinforcement along with SRFC resulted in a significant improvement of the post-cracking behavior as well as

energy dissipation capacity of the beams as compared with the other companion beams.

Recent research was conducted at the American University of Beirut using geogrids as confinement material in reinforced concrete columns [Daou, 2018]. Twenty-eight small-scale column specimens of variable height were prepared for testing under axial monotonic compression loading. The main test variables included the internal confinement (transverse reinforcement or geogrids), geogrid type (uniaxial or biaxial), the number of geogrids layers (1 or 2), and the height to diameter ratio or the aspect ratio  $D/L$  of the section. The intended concrete compressive strength was 11 MPa for all tested specimens. Test results indicated that internal uniaxial geogrid confinement improved the axial load capacity to a level similar to closely spaced ties, whereas biaxial geogrid confinement led to a slight decrease in ultimate strength. However, both types of geogrids led to significant improvement of the axial load-displacement history and energy dissipation which was more than the improvement achieved with closely spaced ties specimens. Two distinct analytical models were developed to predict the load-displacement behavior. The first model showed the behavior of unconfined plain concrete, whereas in the second model, uniaxial and biaxial geogrid behavior were quantified as transverse reinforcement. Comparison between the experimental and analytical results indicated that the models provided satisfactory predictions of the stress-strain response.

## 2.3 External confinement

### 2.3.1 Action of FRP confinement

With Fiber Reinforced Polymer (FRP) confinement, the concrete structural member is latterly confined in a passive nature, and it expands laterally when subjected to axial compression load. The FRP jacket is loaded in tension in the hoop direction due to the expansion of the structure. In steel-confined concrete, the lateral confining pressure is constant following the yielding in steel providing a ductile behavior in contrast with FRP which behaves in a brittle manner. The confining pressure increases with the increase in lateral strain because FRP does not yield. The schematic illustration of the confining action in FRP-confined concrete shown in Figure 2.1 shows that all stresses are in their positive direction. In FRP, tensile stresses and strains are positive. Concrete compression stresses and strains are positive. The radial (lateral) confining pressure acting on the concrete core  $\sigma_r$  is given by:

$$\sigma_r = \frac{\sigma_h t}{R} = \frac{2\sigma_h t}{d} \quad (2.1)$$

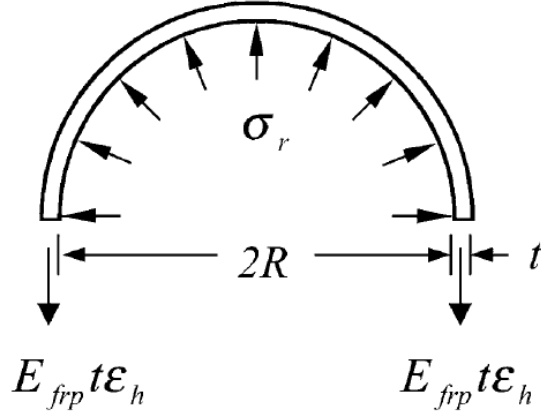


Figure 2.1: Confining action of FRP jacket

where  $\sigma_h$  = tensile stress in the FRP jacket in the hoop direction,  $t$  = total thickness of the FRP jacket, and  $R$  and  $d$  are the radius and diameter of the confined concrete core, respectively. If the FRP is loaded in hoop tension only, then the hoop stress in the FRP jacket  $\sigma_h$  is proportional to the hoop strain  $\epsilon_h$  due to the linearity of FRP [Lam and Teng, 2003] and is given by

$$\sigma_h = E_{frp} \epsilon_h \quad (2.2)$$

where  $E_{frp}$  = elastic modulus of FRP.

### 2.3.2 FRP stress-strain curves type

The most common stress-strain curve of reinforced concrete confined using FRP sheets exhibits a monotonically ascending bi-linear shape if the amount of FRP exceeds a certain threshold as shown in Figure (2.2-a). In this case, the FRP sufficiently confines concrete, and the ultimate stress and strain are reached at the same point simultaneously ( $f'_{cc} = f'_{cu}$ ). A significant enhancement is observed in both ductility and ultimate strength. However, in some tests such bi-linear stress-strain behavior is not achieved and a post-peak descending part is detected where the ultimate stress ( $f'_{cc}$ ) is reached before the FRP jacket is ruptured as shown in Figure (2.2-b). This behavior can result in a stress in concrete at ultimate strain ( $f'_{cu}$ ) which is either smaller or greater than the ultimate strength of unconfined concrete ( $f'_{co}$ ). Figure (2.2-b) shows that adequate FRP confinement enhances the strength of concrete. Also, the compressive strength of the unconfined concrete ( $f'_{co}$ ) is below the ( $f'_{cu}$ ). However, in Figure (2.2-c), the FRP

is considered inadequate, where the stress-strain curve ends at stress ( $f'_{cu}$ ) lower than ( $f'_{co}$ ).

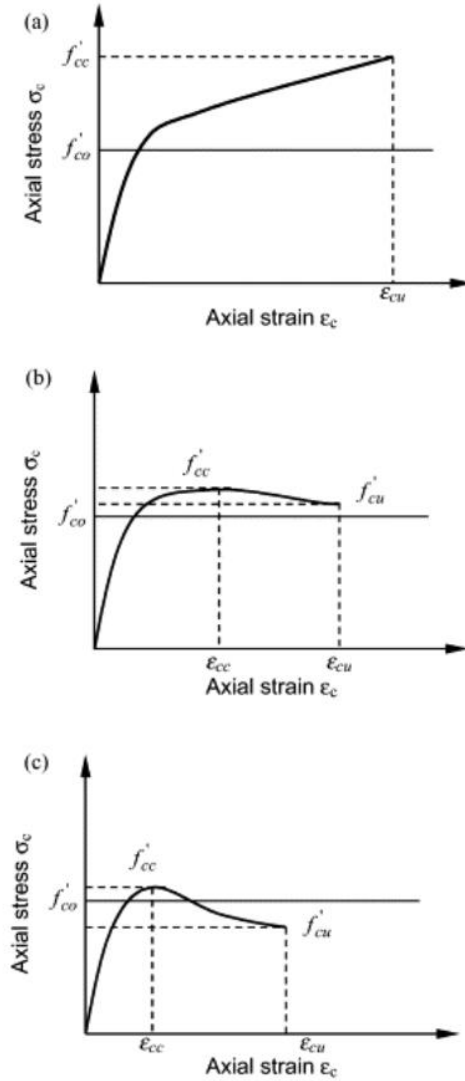


Figure 2.2: Classification of stress–strain curves of FRP-confined concrete. (a) Increasing type; (b) Decreasing type with  $f'_{cu} \geq f'_{co}$ ; (c) Decreasing type with  $f'_{cu} < f'_{co}$ . [Lam and Teng, 2003]

The stress-strain curves with decreasing type are directly dependent on the concrete stress value  $f'_{cu}$  that corresponds to the ultimate strain at the termination of the curve. According to [Lam and Teng, 2003], if  $f'_{cu} > f'_{co}$  (Figure 2.2-b), the confinement is sufficient, but if  $f'_{cu} < f'_{co}$  (Figure 2.2-c), then the confinement is not sufficient, and there is no considerable enhancement in the compressive strength of the confined specimens.

[Lam and Teng, 2003] used the data of 76 specimens confined with carbon, high modulus carbon, aramid, or glass FRP to develop an analysis-oriented model. They found that for circular specimens, the enhancement in the compressive strength of confined concrete should not be expected if the modified confinement ratio (MCR) which is equivalent to  $(f_l/f_{co})$  is less than 0.15 where  $f_l$  is equivalent to the maximum confining pressure and  $f_{co}$  is the compressive strength of unconfined concrete [Mirmiran et al., 1998]. However, according to [Spoelstra and Monti, 1999], if  $f_l/(f_{co})$  is less than 0.07, then the stress of concrete at the ultimate strain  $f_{cu}$  falls below  $f_{co}$  using their analysis-oriented model. Therefore, the stress-strain curve with a descending post-peak branch is expected and no considerable strength enhancement is assumed. However, if  $f_l/(f_{co})$  greater than 0.07, an expected ascending post-peak branch, results in a considerable enhancement in strength ([Lam and Teng, 2003]; [Mirmiran et al., 1998]; [Spoelstra and Monti, 1999]).

### 2.3.3 Reinforced concrete external confinement

[Mirmiran et al., 1998] investigated the use of fiber-reinforced plastic (FRP) as external confinement of concrete columns. They tested a total of 12 square specimens (152.5x152.5x305 mm) and 30 cylindrical specimens (152.5x305 mm) in uniaxial compression using the 2500 kN MTS machine. The main parameters in this study were the length, shape, and bond (adhesive or mechanical) of FRP-confined concrete. The testing results showed that the circular specimens have a higher confinement effect over the square ones, and that the adhesive bond does not affect the load-carrying capacity of the confined FRP specimens. The ranges within 2:1 and 5:1 of the length-to-diameter ratio had limited effect on either strength or ductility of the section. Strength reductions and eccentricities were both within the limits prescribed by the ACI Building Code for tied columns. On the other hand, the mechanical shear connectors significantly increased the load-carrying capacity by distributing the confinement pressure around the circumference of the tube more effectively.

[Pessiki et al., 2001] conducted an experimental study on the use of fiber-reinforced polymer (FRP) composite jackets as external confinement of small-scale square and circular plain concrete specimens and reinforced concrete large-scale square and circular columns. The specimens were tested in a monotonic concentric uniaxial manner using the 5,000-kip capacity Universal Testing machine located in Fritz Laboratory at Lehigh University. They tested sixteen circular (152x610 mm) and twelve square (152x152x610 mm) small-scale plain concrete specimens followed by four circular (508x1830 mm) and four square (457x457x1830 mm) full-scale reinforced concrete specimens. They concluded that FRP jacketing improved the deformation and the axial load-carrying capacities as compared to unjacketed specimens. Moreover, the axial performance of FRP jacketed specimens was found to be significantly influenced by the cross-

sectional geometry since circular specimens were more efficient than square ones.

In another study, [Bournas et al., 2007] investigated the effectiveness of jacketing reinforced concrete columns with limited capacity due to buckling of longitudinal bars. They compared textile-reinforced mortar (TRM) to fiber-reinforced polymer (FRP) sheets having equal stiffness and strength. To achieve this, they tested fifteen short reinforced concrete prisms of dimensions 200x200x380 mm with their four corners rounded at a radius equal to 25 mm, under concentric compression using an MTS testing machine. In addition, another three nearly full-scale non-seismically detailed reinforced concrete columns of dimensions 250x250x1600 mm with the same geometry and reinforcement were subjected to cyclic uniaxial flexure under constant load. The experimental program parameters were the following: the number of layers of TRM and FRP, the internal steel reinforcement, and the spacing of stirrups. The results showed a significant increase in the compressive strength and the deformation capacity of the short prism specimens through delaying the buckling of the longitudinal bars. This gain was enhanced by the increase in the volumetric ratio of the TRM wrap. However, the TRM jacket was around 10% less effective than the FRP jacket, both materials having equal stiffness and strength, in terms of deformation and strength capacity. In addition, the nearly full-scale columns turned out to be very efficient and equal to their FRP counterpart. The energy dissipation and the deformation capacity increased with respect to old-type reinforced concrete columns with poor detailing through delaying buckling of the longitudinal bars.

[Ilki et al., 2008] investigated the use of carbon fiber-reinforced polymer (CFRP) in jacketing circular and rectangular columns with low and medium strength concrete. Sixty-eight reinforced concrete specimens were tested using an Amsler universal testing machine with a capacity of 5,000 kN under monotonic and cyclic uniaxial compressive load. The specimens included twenty-eight medium strength concrete specimens with adequate internal transverse reinforcement, and forty specimens of low strength concrete with inadequate internal transverse reinforcement. Test parameters included the cross-section shape, corner radius, thickness of the CFRP jacket, unconfined concrete strength, amount of internal transverse reinforcement, the existence of pre-damage, type of loading, anchorage details, the bonding pattern orientation, spacing of transverse reinforcement, and additional corner supports of the CFRP sheets. Test results confirmed an increase in ductility and ultimate strength. The circular specimens showed a significant increase in strength while the rectangular specimens experienced a higher ultimate axial deformation without a major loss in strength. Retrofitting was more efficient in lower strength concrete.

In 2017, a research study was conducted at the American University of Beirut using hemp fiber-reinforced polymer (HFRP) as external confinement for concrete columns [Ghalieh et al., 2017]. The research parameters were the following: the columns slenderness ratio, transverse steel reinforcement, and the number of confining layers. Thirty-six specimens were cast and tested in axial compression

using the MTS machine with a constant displacement rate of 3 mm/min. The results showed that HFRP sheets increased the compressive strength when using 1, 2, and 4 layers by 9%, 13%, and 22%, respectively. Moreover, the ductility increased with respect to unconfined specimens by 2.78, 3.95, and 6.98 while using 1, 2, and 4 layers respectively. In addition, the axial compressive strength was enhanced by 17.3% along with an increase in ductility in the case of transverse steel reinforcement specimens. All HFRP jacketed specimens failed by single crack in the sheet. Therefore, the failure mode of HFRP specimen was different from that of carbon or glass FRP, where the de-bonding of the confining layer was considered as the failure mode. Various stress models were considered in this study, yet the “Lam and Teng” predictive model was the best fit for all specimens with an error of less than 5% of the maximum confined strength.

### 2.3.4 Fracture mechanics

Reinforced concrete members experience different types of failure modes. Concrete columns are the most crucial member where their failure can result in total collapse of whole buildings. Therefore, if we assume the loading of a column to be centered with no eccentric loading, the result may be one of the three most common failure modes of reinforced concrete columns: compression dominant flexure failure, shear failure, and combined flexure shear failure.

Figure (2.3a) shows the first and most common type: compression dominant flexure failure. It occurs in high-rise reinforced concrete buildings [Doğan and Arslan, 2016]. When the cross-sectional area of the column is lower than the area required to resist the load applied on the column, both the concrete and steel reach yield stress followed by the failure of the column without any lateral deformation. To overcome this, the column cross-sectional area must be sufficient to ensure the stress is below the specified limit. This type of failure is most likely to be found in relatively shorter columns. It is also called “pure compression” and is mainly experienced in cases of pedestals where the ratio of height to least lateral dimension is less than 3.

The second mode, known as a shear failure and shown in Figure (2.3b), is mainly found in reinforced concrete columns lacking lateral reinforcement. It occurs mostly after inelastic cyclic loading when the degradation in the lateral load capacity happens before yielding in the longitudinal reinforcement due to shear distress [Han et al., 2013].

Finally, the third type, shown in Figure (2.3c) is called buckling failure and is due to elastic instability which occurs when the yielding of tensile steel reinforcement suddenly reduces the stiffness of a column [Sadeghian and Fam, 2015].



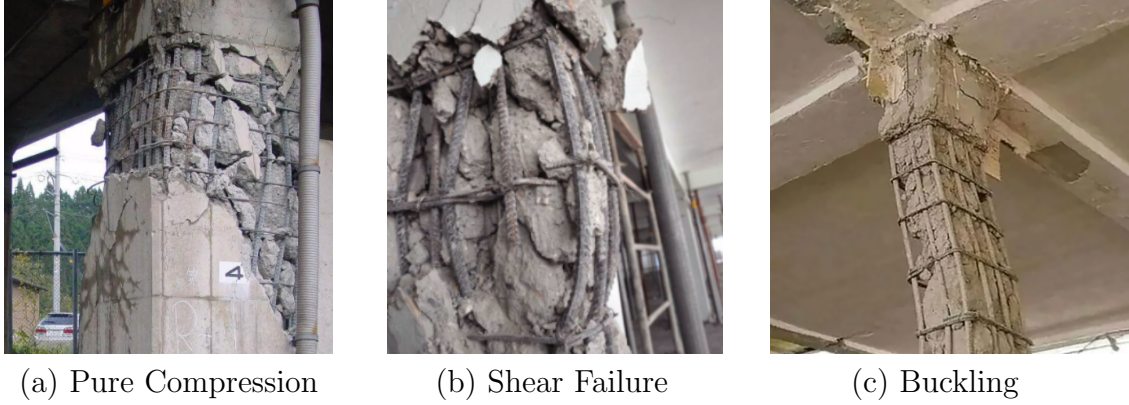


Figure 2.3: Column Failure Modes

### 2.3.5 ACI recommendations

[ACI-440.2R-08, 2002] is the guide for the design and construction of externally bonded FRP systems for strengthening concrete structures. According to [ACI-440.2R-08, 2002], the ACI the maximum confined concrete compressive strength  $f'_{cc}$ , is given by;

$$f'_{cc} = f'_{co} + \psi_f 3.3 \kappa_a f_l \quad (2.3)$$

where,

$f'_{co}$ : unconfined cylinder compressive strength of concrete (MPa).

$\psi_f$ : reduction factor based on the committee judgment  $\varphi = 0.95$ .

$\kappa_a$ : efficiency factor that accounts for geometry of the section. For circular columns  $\kappa_a = 1$ .

The maximum confining pressure,  $f_l$ , provided by an FRP:

$$f_l = \frac{2E_f n t_f \varepsilon_{fe}}{D} \quad (2.4)$$

where,

$E_f$ : tensile modulus of elasticity of FRP (MPa).

$n$ : number of plies of FRP reinforcement.

$t_f$ : nominal thickness of one ply of FRP reinforcement (mm).

$\varepsilon_{fe}$ : effective strain level in FRP reinforcement attained at failure (mm/mm).

$D$ : diameter of compression member of circular cross section, (mm) and the effective strain level in the FRP at failure  $\varepsilon_{fe}$  is:

$$\varepsilon_{fe} = \kappa_\varepsilon \varepsilon_{fu} \quad (2.5)$$

where,

$\kappa_\varepsilon$ : the FRP strain efficiency factor.

$\kappa_\varepsilon$  accounts for the premature failure of the FRP system [Pessiki et al., 2001].

The value of  $\kappa_\varepsilon$  was confirmed by [Spoelstra and Monti, 1999] is 0.55 for circular cross sections using their analytical model.

$\varepsilon_{fu}$ : ultimate strain level in FRP reinforcement attained at failure (mm/mm).

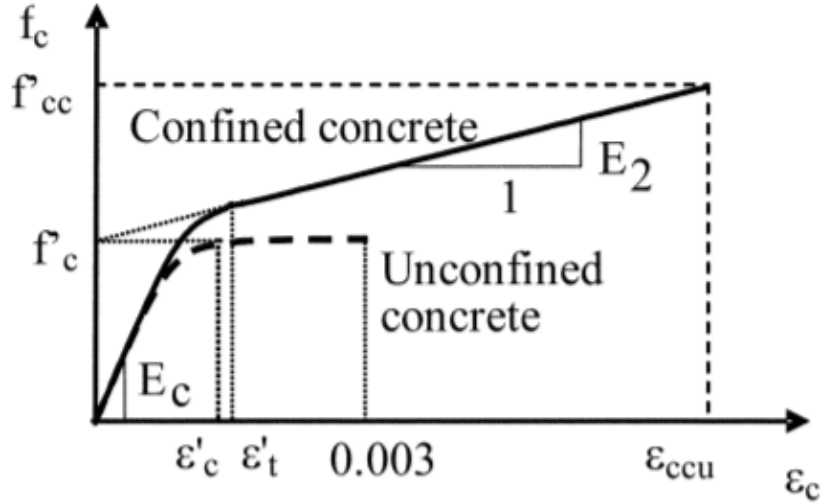


Figure 2.4: Lam and Teng's stress-strain model for FRP-confined concrete [Lam and Teng, 2003]

As recommended by [Lam and Teng, 2003], the ratio of  $f_l/f_c$  should not be less than 0.08 to ensure a sufficient confinement level. The maximum compressive strain in the FRP-confined concrete  $\varepsilon_{ccu}$  can be found:

$$\varepsilon_{ccu} = \varepsilon'_c \left( 1.50 + 12\kappa_b \frac{f_l}{f_c} \left( \frac{\varepsilon_{fe}}{\varepsilon'_c} \right)^{0.45} \right) \leq 0.01 \quad (2.6)$$

The value of  $\varepsilon_{ccu}$  should be less than 0.01 to prevent excessive cracking and the resulting loss of concrete integrity.

where,

$\kappa_b$  is: the efficiency factor accounts for the geometry of the section in the calculation of the ultimate axial strain, for circular cross-section  $\kappa_b = 1.0$ .

Geogrid is an irregular sheet, on contrary to the FRP which is a continuous one. Therefore, an equivalent thickness ( $t_{eq}$ ) is calculated to have a membrane that fully wraps the external surface of the concrete ([Daou et al., 2020]:

$$t_{eq} = \frac{n_l n_r b_r t_r}{h} \quad (2.7)$$

where:

$n_l$ : the number of geogrid layers.

$n_r$ : is the number of ribs.

$b_r$ : is the rib's width.

$t_r$ : is the the rib's thickness.

$h$ : is the specimen's height.

For structural concrete members that have large axial lengths,(Eq. 2.7) becomes:

$$t_{eq} = \frac{n_l b_r t_r}{s_r} \quad (2.8)$$

where:

$s_r$ : is the geogrid ribs spacing.

# Chapter 3

## Experimental Program

### 3.1 Pilot test

Prior to launching an extensive experimental program, it was essential to conduct a pilot test to understand the practicalities and theory behind the use of geogrid as external confinement for reinforced concrete columns. This pilot test introduces some basic concepts such as the set-up characteristics, the failure mechanism of the specimens, and the geogrid efficiency as an externally confining material.

Three small-scale circular column specimens of 240 mm diameter and 500 mm height were cast: a control specimen, an internally confined specimen with biaxial geogrid, and a third specimen externally confined with biaxial geogrid bonded with epoxy. All the specimens were internally reinforced with four 10 mm longitudinal bars and 6 mm stirrups spaced at 20 cm. The specimens were tested using the Tinius Olsen testing machine in uniaxial compression to compare the control and the confined specimens. The methodology used in this testing is discussed in detail in the next subsections. Table 3.1 below shows the pilot test variables.

Table 3.1: Pilot test variables

Specimen Number	Specimen ID	Transverse Reinforcement	Geogrid Confinement	Confinement Location	Number of Layers
1	S20	T6 @200 mm	None	None	None
2	BG-I-1L	T6 @200 mm	Biaxial Geogrid	Internal	1
3	BG-E-1L	T6 @200 mm	Biaxial Geogrid	External	1

### 3.1.1 Geogrid tensile test

A direct tension test was done on the biaxial geogrid sheet used (Tensar SS40). The stress-strain curve for the material is shown in Figure 3.1.

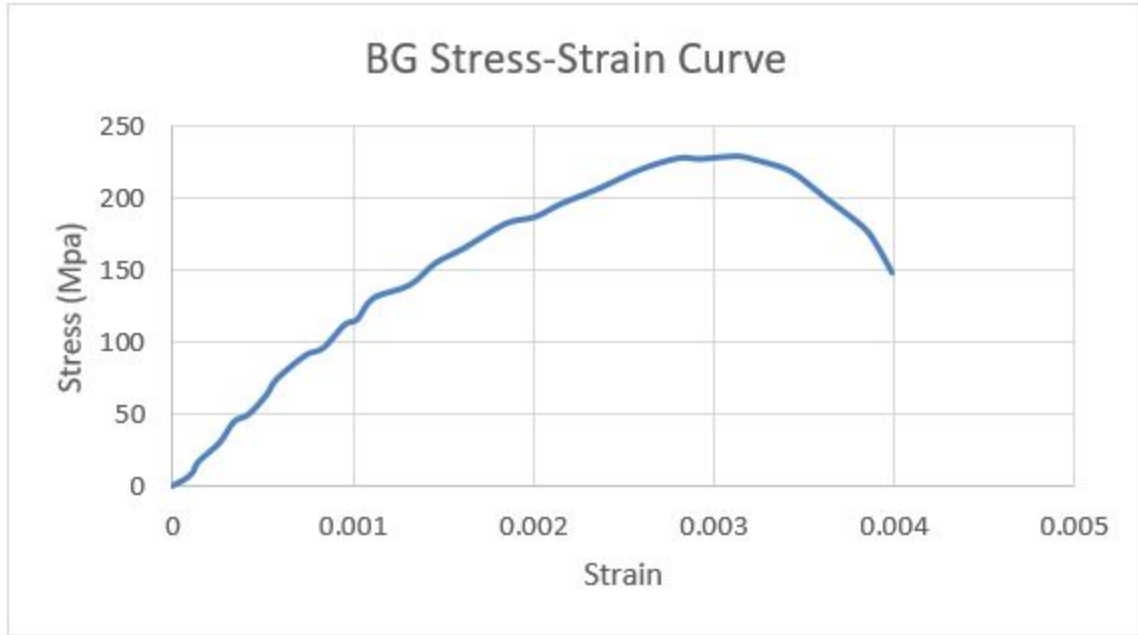


Figure 3.1: Stress-strain curve for the biaxial geogrid [Daou, 2018]

The geogrid used, shown in Figure 3.2, was a stiff, unwoven, punch-drawn geosynthetic material. The properties of the biaxial geogrid were obtained from the manufacturer and are presented in Table 3.2.

Table 3.2: Physical and mechanical properties of the Biaxial Geogrid

Property	Unit	Value
Ultimate Tensile Strength	kN/m	40.0
Load at 2% strain	kN/m	14.0
Load at 5% strain	kN/m	28.0
Approx. Strain at Tult (L/T)	kN/m	11/10
Opening size (L/T)	mm	33/33
Rib width (L/T)	mm	2.2/2.5
Rib thickness (L/T)	mm	2.2/1.4
Junction thickness	mm	5.8

Note: L = Longitudinal direction; T = Transverse direction

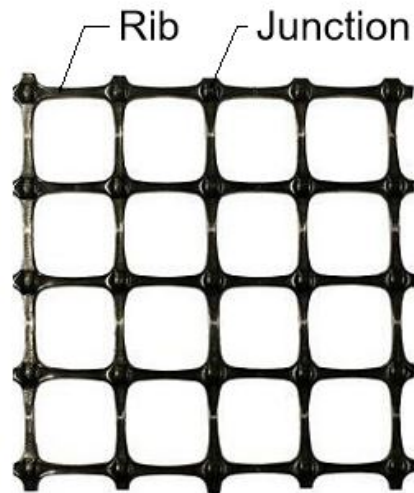


Figure 3.2: Biaxial Geogrid

### 3.1.2 Concrete

The concrete mix consisted of the following batching weights per cubic meter of concrete: 950 kg of small coarse aggregate (9.5mm), 513 kg of natural sand, 437 kg of crushed sand, 270 kg of cement, and 170 kg of water ( $w/c = 0.63$ ), and 3.2 kg of superplasticizer. The intended compressive strength at 28 days was 22 MPa. The cast specimens are shown in Figure 3.3.



Figure 3.3: Pilot test cast specimens

### 3.1.3 Epoxy

Since the experimental program would include specimens externally confined with carbon fiber reinforced polymer sheets (CFRP), it was essential to use the epoxy recommended for CFRP, Sikadur 330. Table 3.3 below shows the properties of the epoxy from the manufacturer.

Table 3.3: Epoxy Properties

Property	Unit	Value
Flexural E-Modulus	MPa	3,800 (7 days at +23°C)
Tensile Strength	MPa	30 (7 days at +23°C)
Tensile Modulus of Elasticity	N/mm <sup>2</sup>	4,500 (7 days at +23°C )
Elongation at break	%	0.9 (7 days at +23°C )
Coefficient of Thermal Expansion	1/°K	4.5 x 10 <sup>-5</sup> (Temperature range -10°C to +40°C)

### 3.1.4 Testing

A uniaxial compression test was conducted using a Tinius Olsen testing machine of 2,000 kN capacity on all the three specimens with a constant rate of 1 mm/min based on [ASTM-C39, 2016]. The samples were axially loaded up to failure. Four linear variable displacement transducers (LVDTs) were aligned using a set-up at a gauge length of 25 cm. Another two LVDTs were aligned externally along the axial direction of the specimen to measure the axial strain. View of the test setup will be shown later in the chapter when discussing the full experimental program. Readings from the four internal LVDTs and the two external LVDTs were averaged to plot the stress-strain curves [ASTM-C39, 2016].

### 3.1.5 Test results

The tested specimens after failure are shown in Figure 3.4. The geogrid specimens confined internally and externally showed a slight decrease in load capacity with respect to the control specimen (S20). However, geogrid confinement led to a significant improvement in the ductility of the load-displacement behavior as indicated by the larger area under the load-displacement curves.



Figure 3.4: Pilot test specimens after testing

## 3.2 Research full experimental program

### 3.2.1 Test Specimens and Test Parameters

Thirty-two small-scale circular column specimens of 240 mm diameter and 500 mm height were prepared for testing using a Tinius Olsen testing machine of 2,000 kN capacity. The main testing variables were: transverse reinforcement spacing, confinement material (Geogrid, Bitumen coated E-glass textile, or FRP), confinement direction (uniaxial or biaxial), number of confinement layers (one or two), confinement location (internal or external). Two replicate specimens were tested for each set of variables to validate the test results. All column specimens were reinforced with four 10 mm longitudinal bars and 6 mm transverse reinforcement or ties with variable spacing. The intended concrete compressive strength was 20 MPa for all specimens except for the one with FRP jacket whose intended strength was set at 12 MPa due to the limited axial load capacity of the testing machine. The test variables are listed below in Table 3.4.



Table 3.4: Test variables

Specimen ID	Compressive Strength (MPa)	Transverse Reinforcement	Geogrid Confinement	Confinement Location	Number of Layers
S20	20	T6 @200 mm	None	None	None
Plain	20	None	None	None	None
S15	20	T6 @150 mm	None	None	None
S10	20	T6 @100 mm	None	None	None
BG-I-1L	20	T6 @200 mm	Biaxial Geogrid	Internal	1
BG-I-2L	20	T6 @200 mm	Biaxial Geogrid	Internal	2
BG-E-1L	20	T6 @200 mm	Biaxial Geogrid	External	1
BG-E-2L	20	T6 @200 mm	Biaxial Geogrid	External	2
BT-E-1L	20	T6 @200 mm	Bitumen Textile	External	1
BT-E-2L	20	T6 @200 mm	Bitumen Textile	External	2
UG-I-1L	20	T6 @200 mm	Uniaxial Geogrid	Internal	1
UG-I-2L	20	T6 @200 mm	Uniaxial Geogrid	Internal	2
UG-E-1L	20	T6 @200 mm	Uniaxial Geogrid	External	1
UG-E-2L	20	T6 @200 mm	Uniaxial Geogrid	External	2
FRP-E-1L	12	T6 @200 mm	FRP	External	1
FRP-E-2L	12	T6 @200 mm	FRP	External	2

## 3.2.2 Material and specimens preparation

### 3.2.2.1 Concrete Material

The concrete mix used consisted of Portland cement Type I, sand, and well-graded coarse aggregate with a maximum size of 9.5 mm. The specimens were cast in four separate batches. The batches were of thirteen, fifteen, five, and ten specimens each as shown in Figure 3.5. The water-cement ratio was calibrated to produce a compressive strength of around 20 MPa for all specimens and 12 MPa for the CFRP jacketed specimens. Batching weights per cubic meter of concrete are shown in Table 3.5. The compressive strength  $f_c$  was calculated by testing standard 150x300 mm cylinders according to [ASTM-C39, 2016]. The average 28-day concrete compressive strengths of the four batches, obtained by testing standard 150x300 mm concrete cylinders, were 22.93, 13.56, 23.6, and 17.5 MPa, respectively.

Table 3.5: Batching weights per cubic meter of concrete for the two concrete mixes used

Material	Unit	Intended $f'_c = 20$ MPa	Intended $f'_c = 12$ MPa
Cement	(kg/m <sup>3</sup> )	84.4	78.1
Water	(kg/m <sup>3</sup> )	170	174
Admixture	(kg/m <sup>3</sup> )	2.7	2.1
Natural Sand	(kg/m <sup>3</sup> )	198.1	198.1
Crushed Sand	(kg/m <sup>3</sup> )	170.7	170.7
Aggregate (4.75-9.5 mm)	(kg/m <sup>3</sup> )	354.5	354.5
Air Content	Unitless	19	22



(a) First Set



(b) Second Set



(c) Third Set



(d) Fourth Set

Figure 3.5: View of all cast specimens

### 3.2.2.2 Geogrid

Geogrid is known for its high tensile strength, which adds shear strength at the interface between the surrounding material and the geogrid [Tang et al., 2008]. As mentioned before, geogrid is a polymeric material and thus has excellent chemical resistance [Das, 2016]. Geogrids pre-tensioned in one direction are called uniaxial geogrids which consist of one-directional thin ribs joined together at thicker junctions; hence, they provide tensile reinforcement in the longitudinal direction of the ribs. On the other hand, geogrids pre-tensioned in two directions are called biaxial geogrids, which consist of two-directional thin ribs joined together at thicker junctions; hence, they provide tensile reinforcement in both

longitudinal and transverse directions. Tables 3.6 and 3.7 below show the physical and mechanical properties of the two types of geogrids that were used in the research as provided by the manufacturer. Also, views of the two types are shown in Figures 3.6 and 3.7.

Table 3.6: Physical and mechanical properties of the Biaxial Geogrid

Property	Unit	Value
Ultimate Tensile Strength	kN/m	40.0
Load at 2% strain	kN/m	14.0
Load at 5% strain	kN/m	28.0
Approx. Strain at Tult (L/T)	kN/m	11/10
Opening size (L/T)	mm	33/33
Rib width (L/T)	mm	2.2/2.5
Rib thickness (L/T)	mm	2.2/1.4
Junction thickness	mm	5.8

Note: L = Longitudinal direction; T = Transverse direction

Table 3.7: Physical and mechanical properties of the Uniaxial Geogrid

Property	Unit	Value
Aperture size MD	mm	235
Aperture size TD	mm	16
Rib width	mm	6
Rib thickness	mm	1.5
Mass per unit area	g/m <sup>2</sup>	650
Strength at 2% strain	kN/m	28
Strength at 5% strain	kN/m	57
Peak tensile strength	kN/m	88
Yield point elongation	%	10
Junction strength	kN/m	84
Long term design strength	kN/m	39.37

MD: Main direction TD: Transverse direction

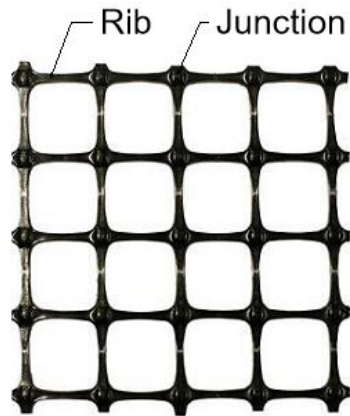


Figure 3.6: Biaxial Geogrid

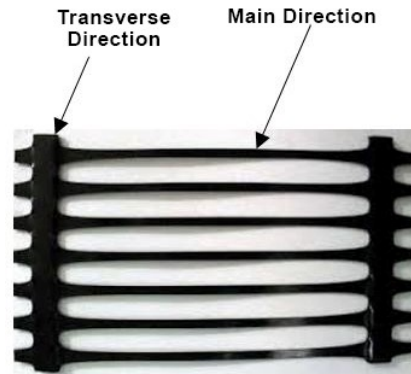


Figure 3.7: Uniaxial Geogrid

### 3.2.2.3 Bitumen coated E-glass textile

The bitumen coated E-glass textile used had a comparable ultimate tensile strength to the stiff geogrid used. The mechanical properties of the selected textile are shown in Table 3.8 below. Also, views of the bitumen coated E-glass textile used is shown in Figures 3.8.



Figure 3.8: Bitumen coated E-glass textile

Table 3.8: Mechanical properties of the bitumen coated E-glass textile [Harajli et al., 2010]

Property	Unit	Value
Weight	$g/m^2$	290
Grid spacing	mm	25
Net grid spacing	mm	23
Rib width	mm	4.5
Rib thickness	mm	0.8
Tensile strength	kN/m	54
Rupture strain	%	2.9
Elastic modulus	GPa	70

### 3.2.2.4 Tensile testing of the geogrids

A tensile test was done on the uniaxial geogrid and biaxial geogrid to get its stress-strain curves shown in Figure 3.8. The tensile testing was conducted using the UTM testing machine following the [ASTM-D6637/D6637M-15, 2021] standards, as shown in the Figure 3.9. The stress-strain curves are shown in Figure 3.10. The ultimate stress, strain, and modulus of elasticity will be used later in defining the behavior of the analytical model.



Figure 3.9: Tensile testing of the geogrid and bitumen textile sheets

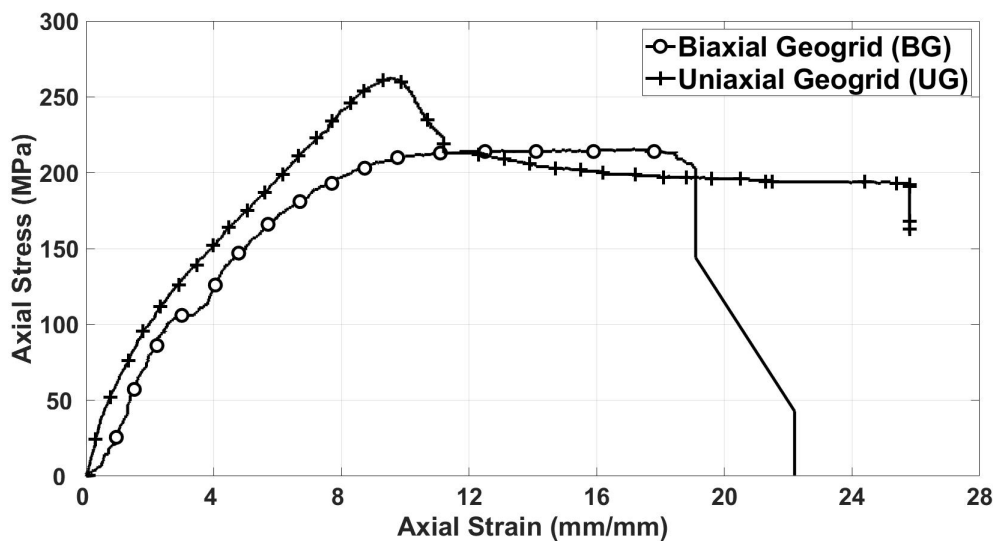


Figure 3.10: Tensile testing stress-strain curve for biaxial and uniaxial geogrid

### 3.2.2.5 Carbon fiber reinforced polymer (CFRP)

For the specimens with external carbon fiber reinforced polymer (CFRP) confinement, the CFRP sheet used was SikaWrap-230 C whose properties are listed in Table 3.9.

Table 3.9: Properties of the CFRP SikaWrap - 230 C

Property		Unit	Values
Dry Fiber Properties	Density	g/cm <sup>3</sup>	1.82
	Thickness	mm	0.129 (based on fiber content)
	Tensile Strength	MPa	4,000 (ISO 10618)
	Elasticity in Tension	N/mm <sup>2</sup>	230,000 (ISO 10618)
	Elongation at break	%	1.7 (ISO 10618)
Laminate Properties	Thickness	mm	0.129
	Tensile Resistance	kN/m	452 (ASTM D 3039*)
	Tensile E-modulus	MPa	220 (ASTM D 3039*)

### 3.2.2.6 Epoxy

The epoxy recommended for bonding the CFRP to concrete was also used to bond the geogrids and the bitumen coated E-glass textile sheets. It is Sikadur 330. The properties of the epoxy as given by the manufacturer were shown in Table 3.3 above.

### 3.2.2.7 Reinforcing steel

All specimens were reinforced with four Grade 60 deformed 10 mm diameter longitudinal bars, while the stirrups were 6 mm diameter Grade 40 bars. Two coupons of each of the two bar sizes used (6 and 10 mm) were tested using the Universal Testing Machine (UTM) to determine the yield strength and the ultimate strength. The values are listed in Table 3.10. The longitudinal reinforcing bars were cut 10 mm short from the top and bottom of the column specimen as shown in Figure 3.11.

Table 3.10: Mechanical characteristics of the steel bars

Properties	Unit	Bar 6 mm	Bar 10 mm
Yield stress ( $f_y$ )	MPa	430	570
Ultimate stress ( $f_u$ )	MPa	510	640

### 3.2.2.8 Formwork setup and preparation of specimens

The forms were installed in to insure that the clear concrete cover to the main reinforcing bars in the transverse direction is 30 mm for the internally tied and externally confined geogrid specimens (Figures 3.11a and 3.11c). As for the internally confined geogrid specimens, the geogrid overlap length was one-half the parameter length to ensure the anchorage of the geogrid sheet. Therefore, due to the geogrid sheet thickness, the clear cover to the longitudinal reinforcing bars decreased from 30 to 26.25 mm for the one layer internally geogrid confined specimens and to 22.5 mm for the two layer geogrid specimen (refer to Figure 3.11b). The geogrid overlap length for the internally and externally confined geogrid specimens was also one-half the parameter length.

The specimens were cast using three separate batches provided by a local Ready-Mix plant (Zoughaib, Beirut, Lebanon) and one batch manually prepared at the Materials Lab of the American University of Beirut (AUB). The batching weights were given in Table 3.5 above. An internal vibrator was used to consolidate the concrete mixes in the forms. The concrete had good workability (slump = 150 mm). After stripping the forms, no honeycombing was observed in all specimens, even those confined internally with geogrids. After casting, all column specimens were covered with wet burlap for 28 days and the accompanying 150x300 mm cylinders were placed in the curing room. This step was necessary to maintain the specimens under moist conditions. The forms were stripped 7 days after casting but the specimens remained covered with wet burlap for the remaining 21 days. The preparation technique used is shown in Figure 3.12 below.

### 3.2.2.9 Capping

The column specimens and the standard cylinders were capped with Sulphur, as specified in [ASTM-C617/C617M, 2012]. The specimen capping was done to provide a smooth and flat surface and to ensure that the top and bottom surfaces are orthogonal to the loading axis.

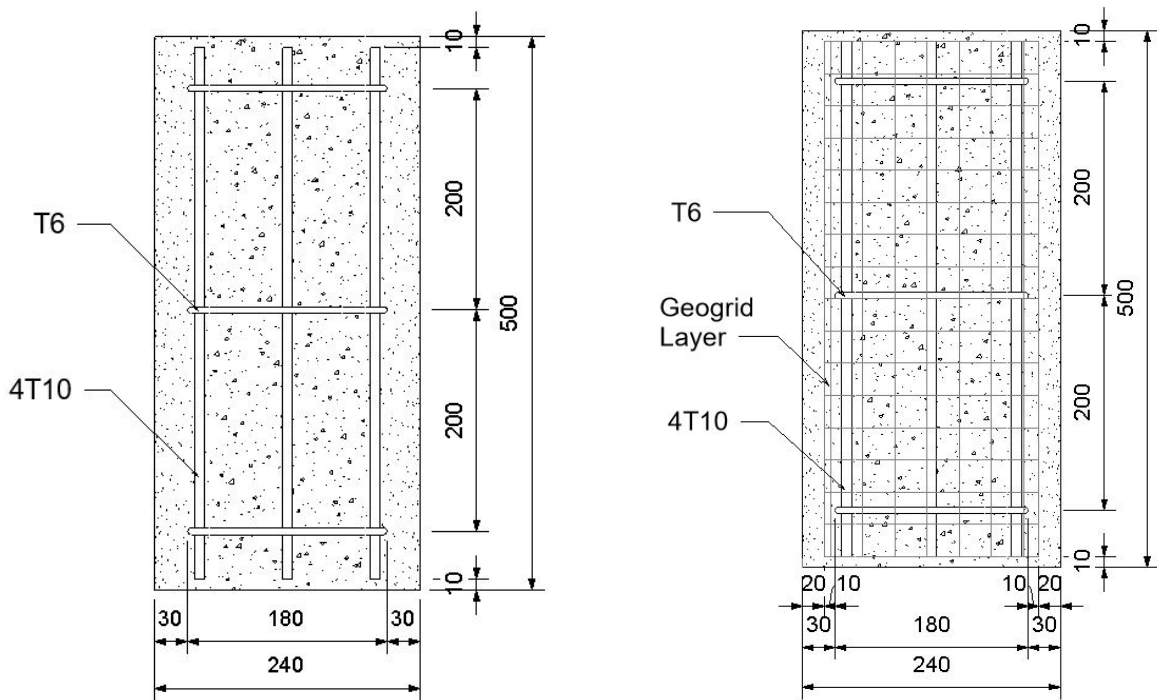
### 3.2.2.10 Instrumentation and testing

The specimens were tested in displacement control at a slow rate using a 2,000 kN capacity 4-column universal Tinius Olsen testing machine. The displacement level was increased in prescribed increments until specimen failure. The axial strain was measured using six linear variable differential transducers (LVDTs) supplied by Omega Engineering, Stamford, Connecticut. Average axial strains were measured using four LVDTs attached to the specimen on either side and positioned over a gauge length of 250 mm in the central portions of the specimens. They were measured over the full height of the specimens using two LVDTs attached between the actuator head and the specimen support giving a gauge length of 500 mm. A steel mounting frame was fabricated at the AUB shops to

support the four internal linear variable differential transducers (LVDTs) at a gauge length of 250 mm, which is half the specimen length as shown in Figure 3.13a. The frame was perfectly aligned using level meter as shown in Figure 3.13b.

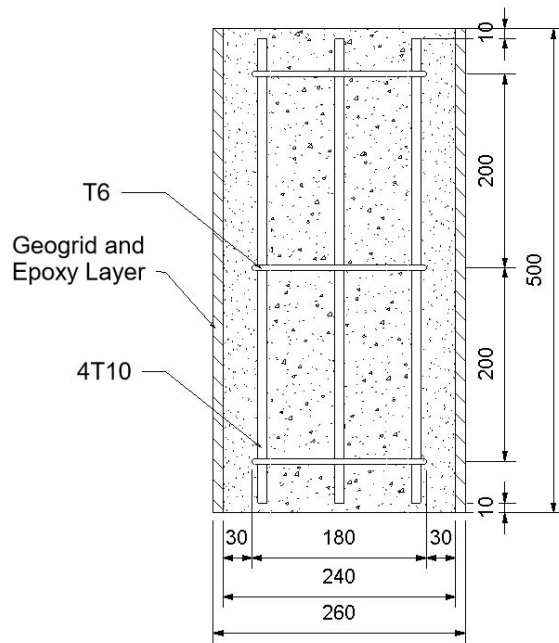
The load was applied at an approximate average rate of 1 mm/min. A computerized data acquisition system monitored all the data including load applied and LVDT readings. A schematic diagram of the test setup is shown in Figure 3.14 and an actual view of the testing machine is shown in Figure 3.15.





(a) Specimen without geogrid

(b) Specimen with internal geogrid



(c) Specimen with external geogrid

Figure 3.11: Schematics of the test specimens



(a) Specimen form



(b) Curing with wet burlap

Figure 3.12: Specimens preparation



(a) Testing Setup



(b) Setup Calibration

Figure 3.13: LVDT's mounting frame

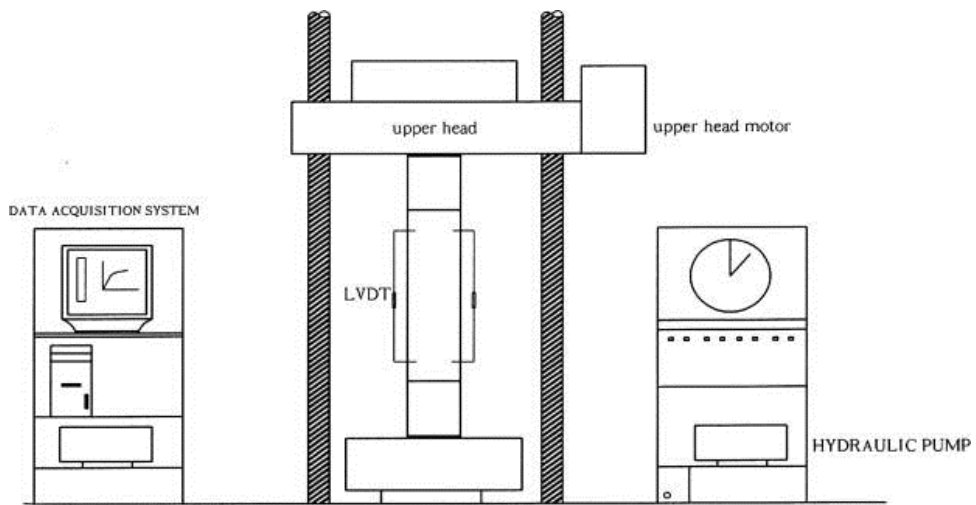


Figure 3.14: Schematic diagram of the test setup

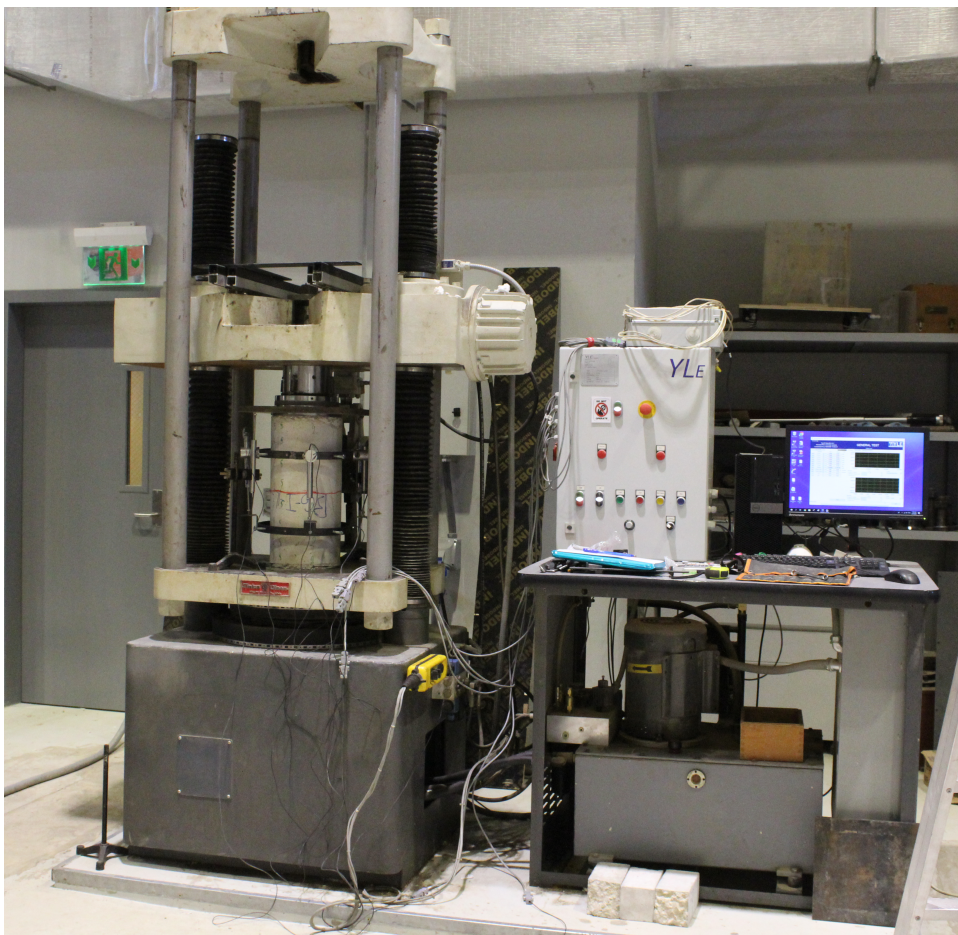


Figure 3.15: Actual view of the testing machine

# Chapter 4

## Test Results and Analysis

As mentioned in Chapter 3, 16 small-scale circular column specimens with different variables were tested. At least two replicates were tested for each set of variables to check the validity of the test results. The variables included the spacing of transverse reinforcement (stirrups), confinement material (Geogrid, Bitumen coated E-glass textile, or FRP), geogrid type (biaxial or uniaxial), number of confining layers (one or two), and confinement location (internal or external). In this chapter, the effect of each variable on the mode of failure and on the test results will be presented and analyzed.

### 4.1 Mode of failure

After testing all specimens including those confined internally or externally with stirrups or geogrids or FRP sheets or bitumen textile sheets, the different modes of failure that were encountered are presented in the following sections.

#### 4.1.1 Specimens internally confined with ties

In the internally confined specimens with various transverse reinforcement spacing, two failure modes were observed. In the first mode, longitudinal cracks developed on the concrete outer surface accompanied by buckling in the longitudinal steel bars in the control specimens S20 having 200 mm transverse reinforcement spacing as shown in Figure 4.1.a. The second mode (pure compression) involves the same pattern of longitudinal cracks but with less reduced buckling in the longitudinal bars. This type was found in the specimens with 150 mm and 100 mm transverse reinforcement spacing and is shown in Figures 4.1.b and 4.1.c. The absence of significant buckling is most likely due to the additional confining ties allowed by the smaller spacing.

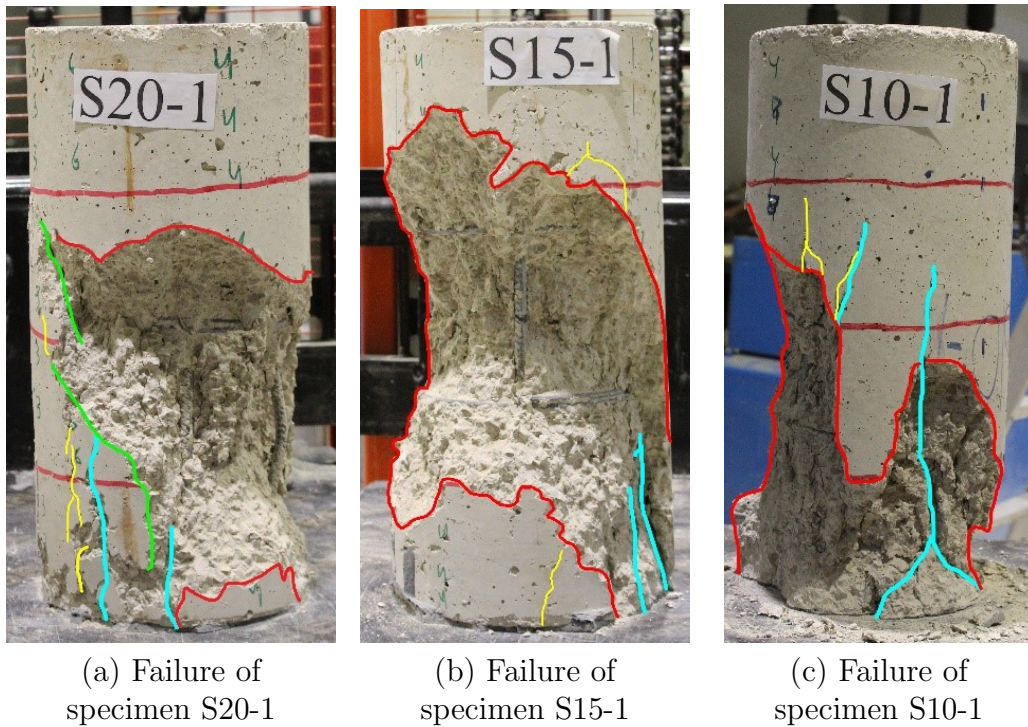


Figure 4.1: Failure of specimens with different transverse tie spacing

#### 4.1.2 Specimens internally confined with uniaxial or biaxial geogrids

Uniaxial and biaxial geogrids are the only internal confinement material used in this research. The failure mode observed was similar to the observations made by [Daou, 2018]. The cracks expanded from the outer surface as longitudinal cracks to the core area of the specimen. Noisy ruptures in the geogrid sheets followed along with bending in the sheets themselves. The failure of the specimen occurred when most of the concrete cover spalled off the geogrid layer exposing the core. In addition, the geogrid sheet anchorage provided by the overlap was lost as shown in Figure 4.2. The spalling of the concrete cover was faster and hence the de-bonding between the concrete cover and the geogrid sheets was more excessive in the case of double layer geogrid specimen due to the smaller concrete cover resulting from using double layers of geogrids. No signs of buckling of the longitudinal bars of the specimens were noted.

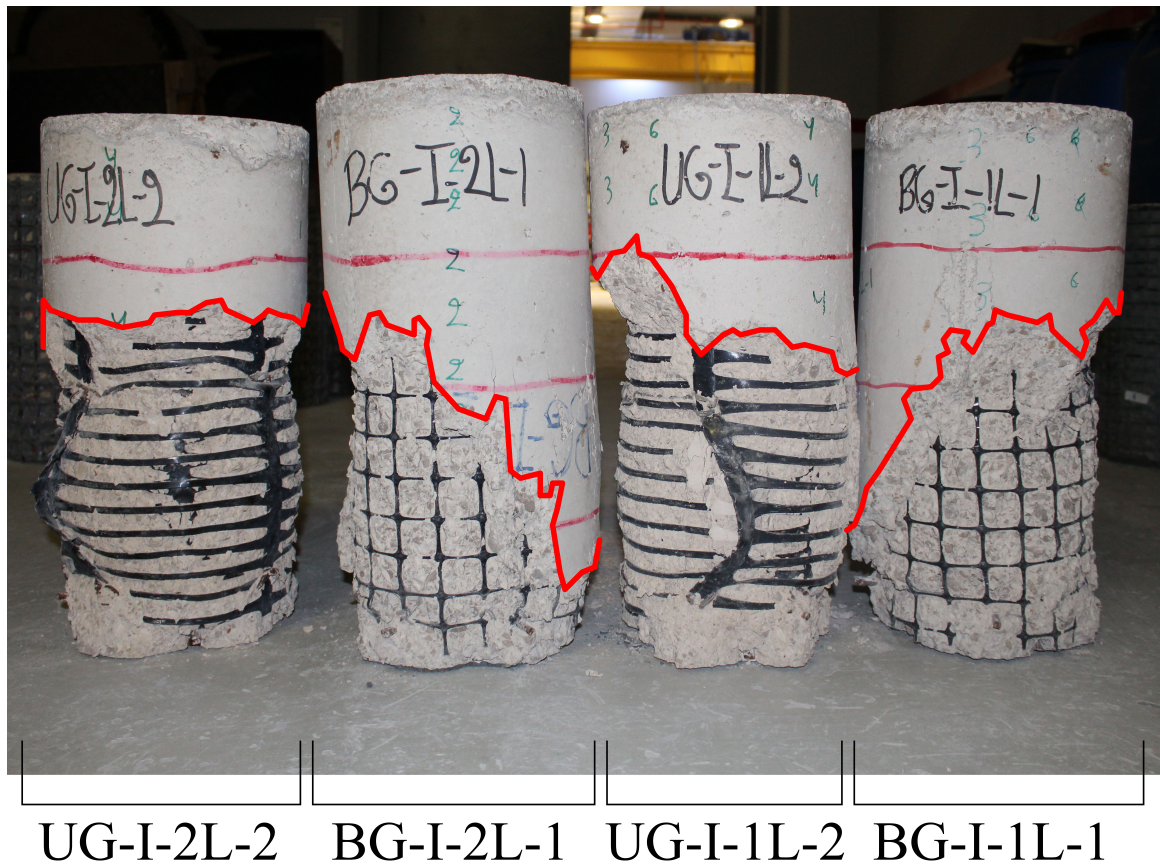


Figure 4.2: Failure modes of the specimens internally confined using biaxial and uniaxial geogrid

### 4.1.3 Specimens with external confinement

#### 4.1.3.1 Using Biaxial and Uniaxial Geogrids

Failure of specimens confined externally with biaxial and uniaxial geogrid sheets was ductile where the specimens exhibited significant displacements with respect to its original length. This displacement was accompanied by popping noise from the epoxy layer followed by excessive crushing in the concrete from the surface to the core. The concrete crushing resulted in deformation and fracture in the geogrid sheet as shown in Figure 4.3.



BG-E-2L-2 UG-E-2L-2 BG-E-1L-1 UG-E-1L-1

Figure 4.3: Failure modes of specimens externally confined using biaxial and uniaxial geogrid

#### 4.1.3.2 Using bitumen textile sheets

The bitumen textile confinement failed by the development of multiple longitudinal cracks in the sheet accompanied by crushing in the concrete as seen in Figure 4.4. The failure mechanism of these specimens is considered as a semi-ductile one, where the specimen exhibited significant displacement before failing through the rupture of the bitumen sheet.

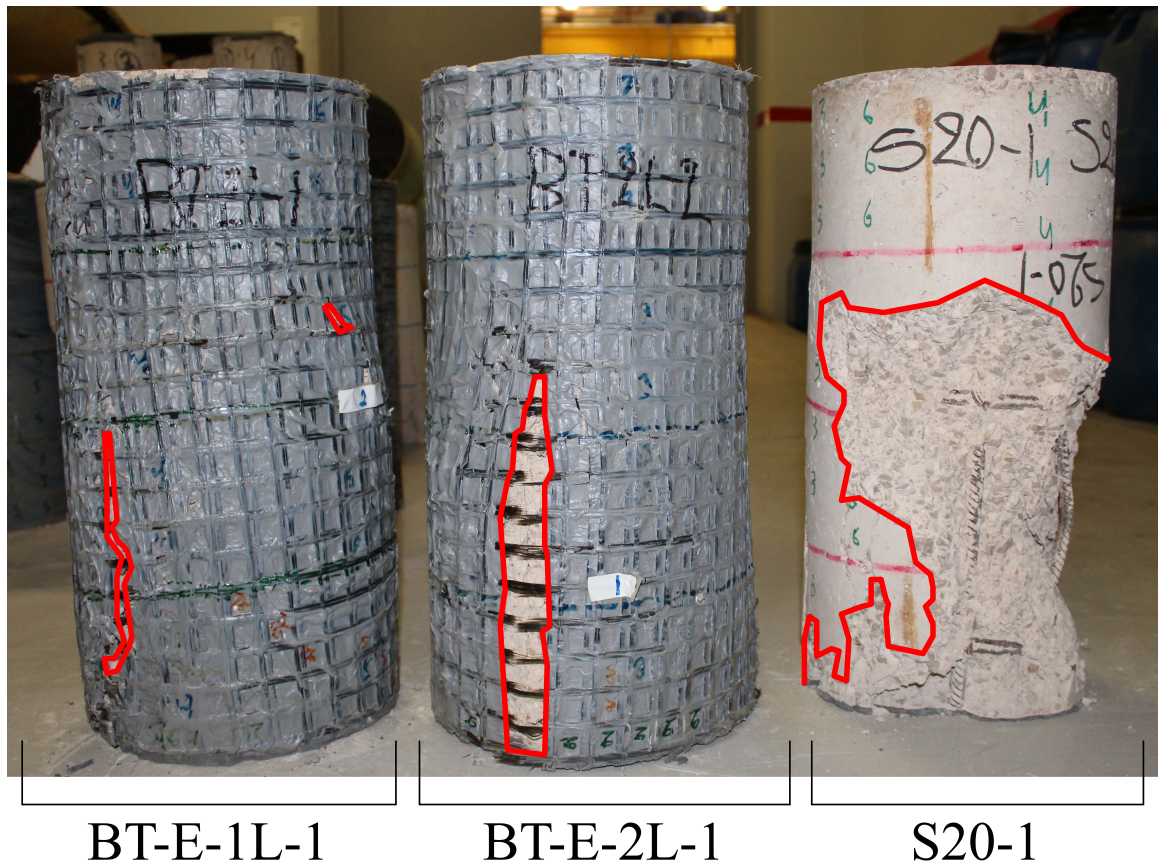


Figure 4.4: Failure modes of the specimens externally confined using bitumen textile sheets

#### 4.1.3.3 Using FRP sheets

The FRP jacketed specimens failed by the development of a sudden single or multiple ring rupture in the confining layer as shown in Figure 4.5. The rupture was accompanied by a loud popping noise indicating the brittle behavior of the FRP jacket. The concrete core of the confining layer was fully crushed indicating the failure of the concrete happened before the rupture of the FRP confining layer.



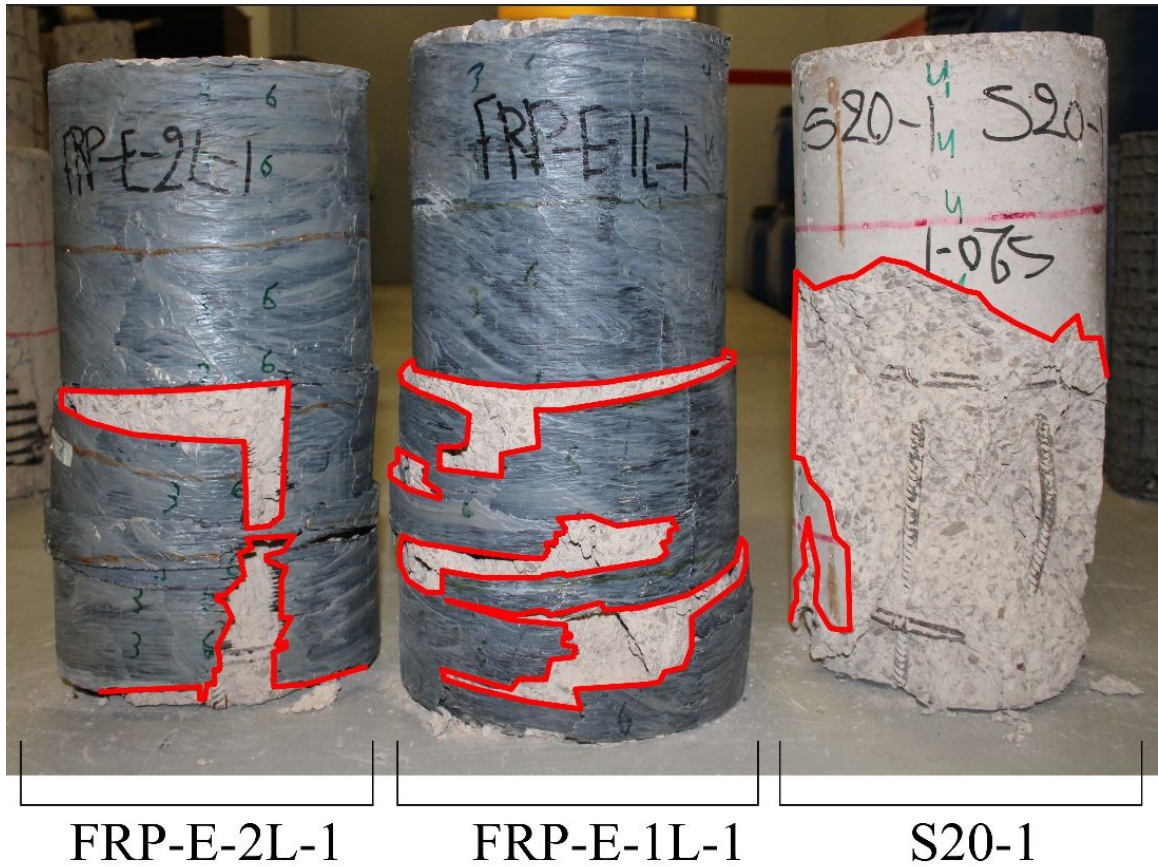


Figure 4.5: Failure modes of specimens externally confined using FRP sheets

## 4.2 Test result and analysis

Test results shown in the Table 4.1 indicate the average value of all tested replicates of a specific specimen. The results include: the measured ultimate axial load applied  $P_{max}$  normalized at a common concrete compressive strength of 20 MPa, the ratio  $\alpha$  of the ultimate load relative to the control specimen S20, the axial deformations  $\delta_y$  and  $\delta_f$ , the displacement ductility index  $\mu$  ( $\mu = \delta_f / \delta_y$ ), fracture energy  $F$ , and the energy ductility index  $K$  which is the ratio of fracture energies relative to the control specimen S20.

The schematic load-displacement curve shown in Figure 4.6 defines  $\delta_y$ ,  $\delta_f$ , and  $F$ : the axial displacement  $y$  corresponds to the yield load  $P_y$  ( $P_y = 0.7P_{max}$ ) at which the load-displacement curve shifts from a linear to a non-linear stage, the axial displacement  $\delta_f$  is measured at one-half the maximum load  $P_{max}/2$ , and the fracture energy  $F$  is calculated as the area under the load-displacement curve up to  $\delta_f$ . The values of  $\alpha$ ,  $\mu$ , and  $K$  are also presented in Figures 4.7, 4.8, and 4.9, respectively.

Ductility is the ability of an element or structural system to undergo in-

elastic deformation without substantial loss in resistance. In this study, two indicators were used to measure the ductility of the load-displacement history. The first indicator is the displacement ductility index ( $\mu$ ), also known as the ratio of axial deformations. The second indicator is the energy ductility index K, measured as the ratio of fracture energy F of the specimen with respect to the control specimen S20.

Table 4.1: Test Results

Specimen ID	Normalized ultimate load $P_{max}$ (kN)	Ratio of ultimate loads $\alpha+$	$\delta_{y++}$	$\delta_{f++}$	Displacement ductility index $\mu+++$	Fracture energy F (N-m)	Energy ductility index $K++++$
S20***	694	1.00	0.163	2.052	12.59	1082	1.00
Plain*	649	0.93	0.137	1.832	13.35	911	0.84
S15*	715	1.03	0.154	3.541	22.97	1909	1.76
S10*	832	1.20	0.156	1.982	12.70	1193	1.10
BG-I-1L*	783	1.13	0.173	4.346	25.06	2364	2.19
BG-I-2L**	738	1.06	0.304	7.557	24.86	4256	3.93
BG-E-1L**	794	1.14	0.283	3.817	13.51	2218	2.05
BG-E-2L**	820	1.18	0.174	6.610	37.93	3928	3.63
BT-E-1L*	902	1.30	0.189	4.454	23.52	2847	2.63
BT-E-2L*	897	1.29	0.189	2.637	13.97	1984	1.83
UG-I-1L*	747	1.08	0.149	5.612	37.66	2734	2.53
UG-I-2L*	712	1.03	0.189	10.036	53.17	4407	4.07
UG-E-1L*	786	1.13	0.167	18.544	110.79	8080	7.47
UG-E-2L*	849	1.22	0.197	19.902	101.09	9191	8.49
FRP-E-1L*	1414	2.04	0.703	3.191	4.54	6719	6.21
FRP-E-2L*	1926	2.78	2.036	10.704	5.26	13272	12.27

\*Two replicates for this specimen were tested to validate the test results.

\*\*Three replicates for this specimen were tested to validate the test results.

\*\*\*Four replicates for this specimen were tested to validate the test results.

$+\alpha$  is the ratio of the ultimate load of the tested specimen to that of the control specimen S20.

$++\delta_y$  and  $\delta_f$  are defined in Figure 4.6.

$+++ \mu$  is the displacement ductility index and is calculated as the ratio of  $\delta_f$  to  $\delta_y$ .

$++++K$  is the energy ductility index and is calculated as the ratio of the fracture energy of the tested specimen divided by that of the control specimen S20; fracture energy F is defined in Figure 4.6.

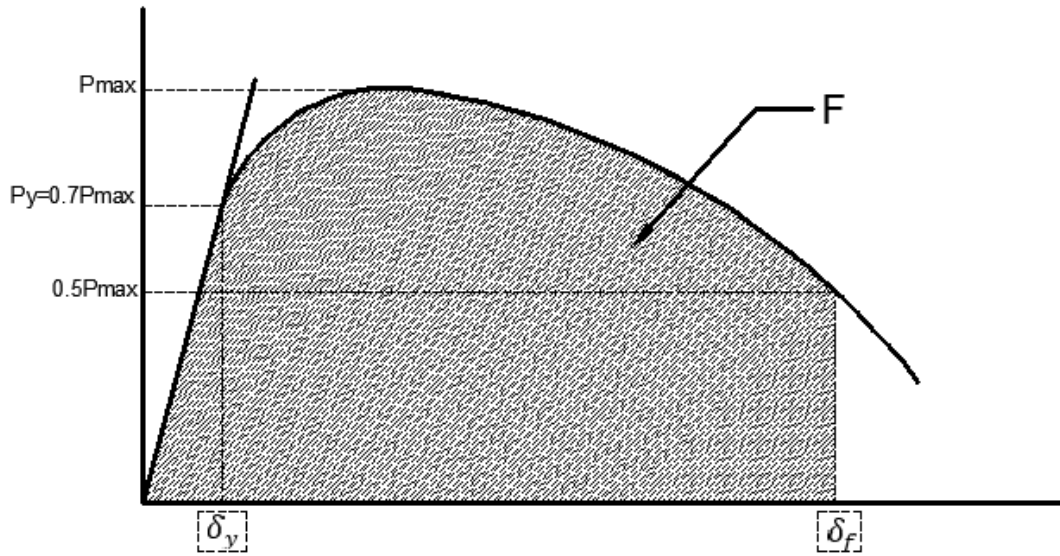


Figure 4.6: Schematic load-displacement curve to define the parameters used in Table 4.1

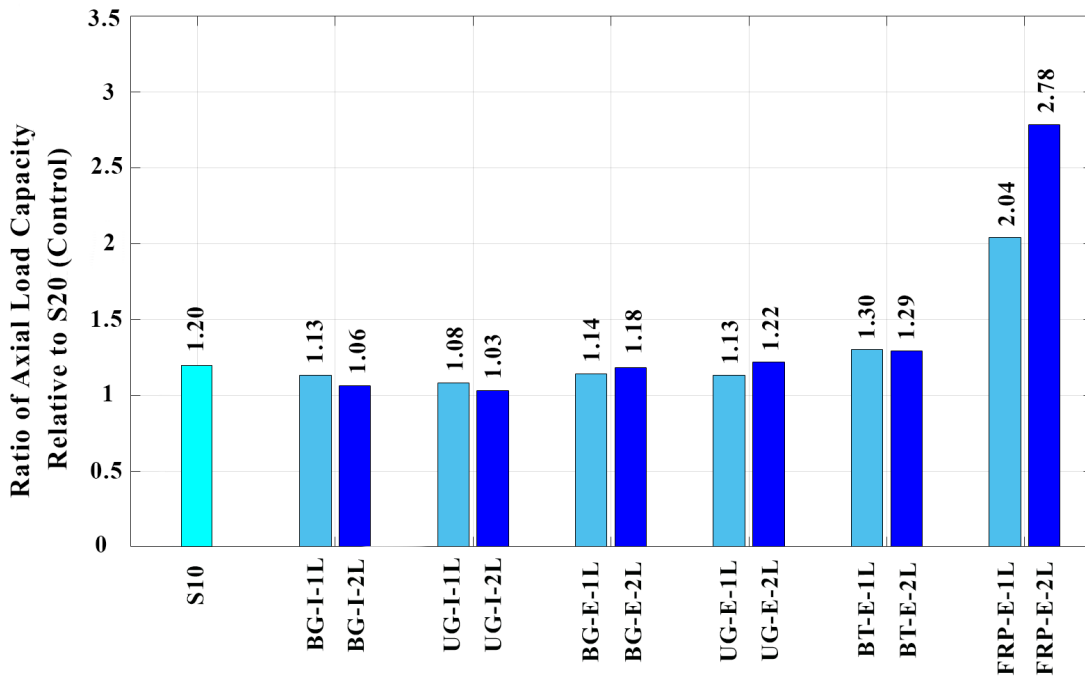


Figure 4.7: Ratio of ultimate axial load capacity values of all tested specimens relative to S20

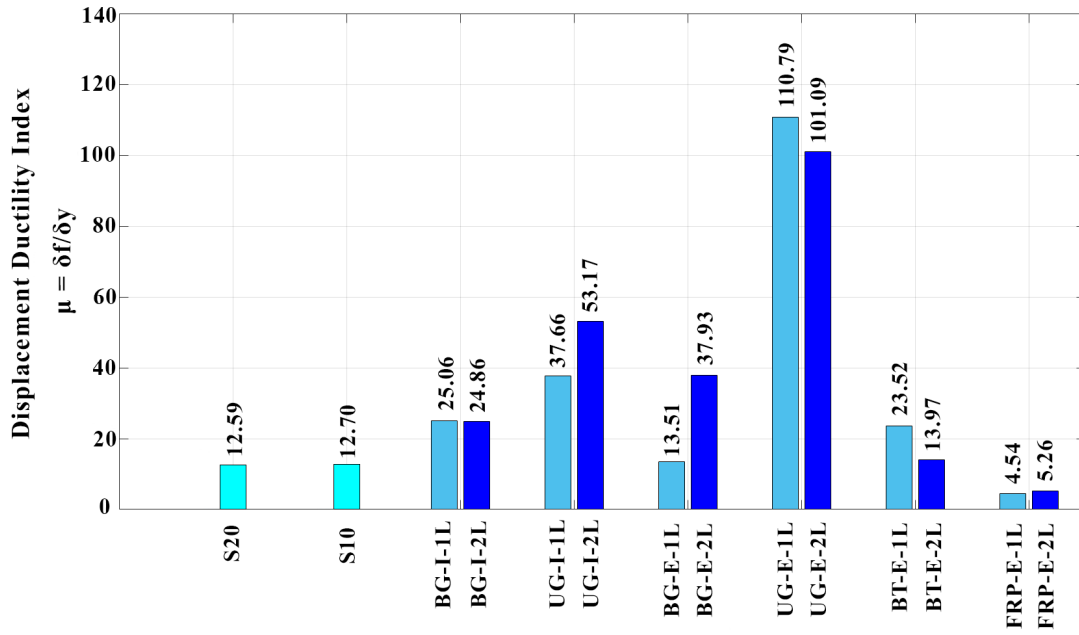


Figure 4.8: Average displacement ductility index values of all tested specimens

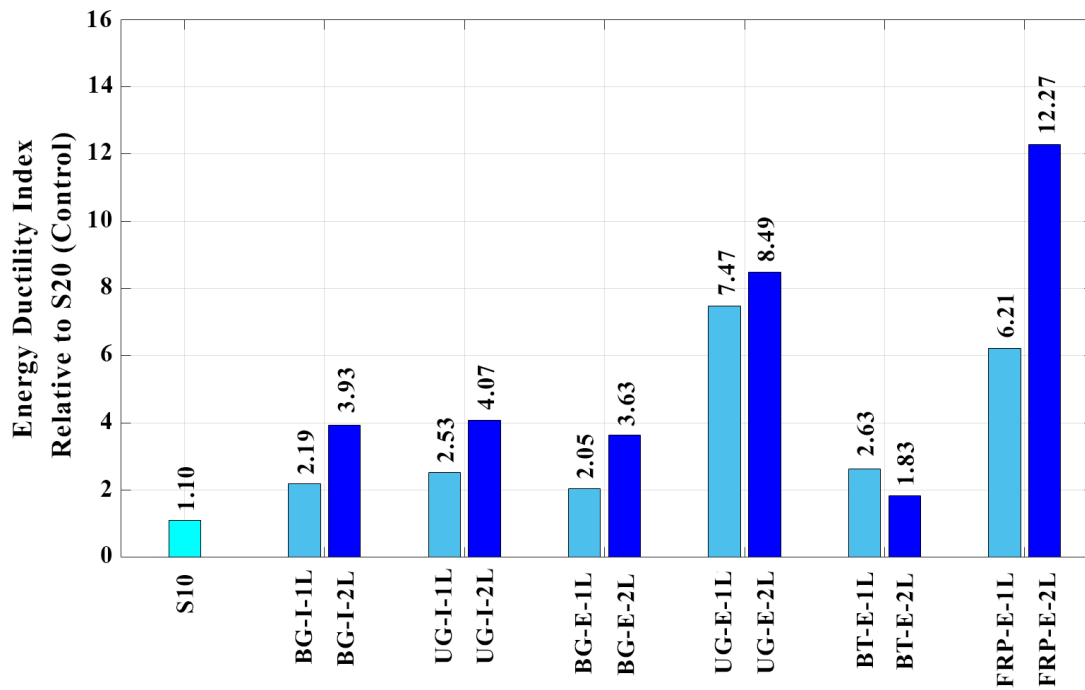


Figure 4.9: Average energy ductility index values of all tested specimens

### 4.2.1 Effect of the stirrups spacing

Specimens S20, S15, and S10 had tie spacing of 200, 150, and 100 mm, respectively. Referring to Table 4.1 and Figure 4.7, the ultimate load capacity of S10 improved by around 20% relative to the control specimen S20, whereas the increase in S15 was only 3%. The Plain specimen with no stirrups recorded 7% less strength than S20. The load-axial displacement curves shown in Figure 4.10 indicate the positive effect of stirrup confinement on load-displacement history beyond the ultimate load capacity. Values of both ductility indices,  $\mu$  and  $K$ , listed in Table 4.1 and shown in Figures 4.8 and 4.9, indicate that the use of small stirrup spacing had a positive effect on the ductility of the specimens as compared to the control specimen S20.

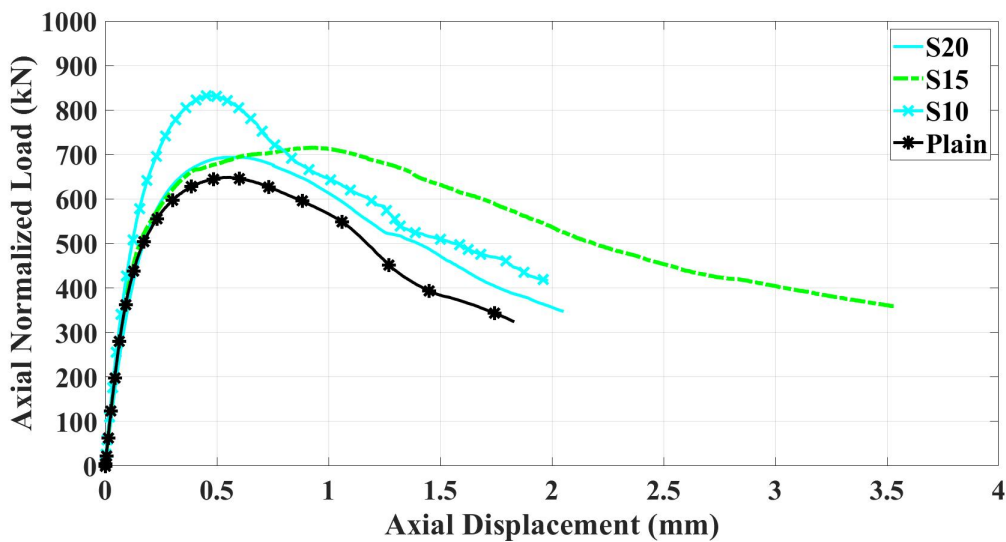


Figure 4.10: Load-displacement curves for specimens with different stirrup spacing

### 4.2.2 Effect of confinement type

#### 4.2.2.1 Internal Confinement

Failure of specimens with no or poor internal confinement (Plain and S20) was preceded by crushing of the concrete and full buckling of the longitudinal steel bar. The presence of closely spaced stirrups or any of the two types of geogrid sheets (uniaxial or biaxial) provided significant confinement to the concrete core and prevented buckling of the steel longitudinal bars.

The positive effect of internal confinement on the mode of failure was also reflected in the load-displacement history. Figure 4.11 shows the load-displacement curves of specimens internally confined using stirrups, biaxial geogrids (one and

two layers), and uniaxial geogrids (one and two layers). It can be seen that the initial stiffness of the load-displacement curve of S10 is greater than all other geogrid specimens. Whereas the 10 mm stirrup spacing (S10) improved the load capacity by 20% relative to S20, the improvements using biaxial geogrids were 13% for one layer (BG-I-1L) and 6% for two layers (BG-I-2L), and were 8% for one layer (UG-I-1L) and 3% for two layers (UG-I-2L) of uniaxial geogrids (refer to Table 4.1 and Figure 4.7). The lower axial load capacity of the two layers internal geogrid specimens, biaxial and uniaxial, relative to the single layer specimens could be referred to the faster spalling of the relatively smaller concrete cover. As mentioned in Section B.2.5 of Chapter 3, the concrete cover of the single and double-layered specimens were 26.25 mm and 22.5 mm, respectively, and thus de-bonding between the concrete cover and the geogrid sheets was more excessive in the case of double layer geogrid specimen in the failure mechanism.

The ultimate load superiority of the specimen with closely spaced ties (S10) is not extended to ductility of the load-deflection history as indicated by the two ductility indices listed in Table 4.1 and by the significant increase in energy dissipation before specimen rupture as shown in Figure 4.11. The displacement at maximum load and the fracture energy were greater for the geogrid specimens than for the closely spaced tie specimen S10. With reference to Table 4.1 and Figures 4.8 and 4.9, the displacement ductility indices were 12.7 for S10, around 25 for the two biaxial geogrids specimens (single layer and double layer), and reached 53.17 for the two layers uniaxial geogrid specimen. Whereas the 10 cm tie spacing improved the fracture energy relative to S20 by 10%, the improvements were 119% and 293% for the one and two layers of internal biaxial geogrids and were 153% and 307% for the one and two layers of internal uniaxial geogrids, respectively. The ductility superiority of the geogrid specimens to the tie confined specimens is related to the continuous confinement provided by the geogrid to the concrete core.

Although the double layer geogrid specimens had lower axial load capacity than the single layer specimens, however they allowed significant increase in the axial displacement at failure and therefore had larger fracture energy. Also, the larger values of the ductility indices of the uniaxial geogrid specimens as compared to the biaxial geogrid specimens could be related to the higher tensile strength of the uniaxial geogrid used in the research program allowing it to sustain larger tensile stresses before rupture (refer to Tables 3.6 and 3.7 of Chapter 3). In addition, the aperture of the biaxial geogrid and uniaxial geogrid is 30 mm and 16 mm respectively between two consecutive ribs, refer to Section 3.2.2.2 in Chapter 3, which by substitution increase the number of ribs per specimen, thus increase the ductility.

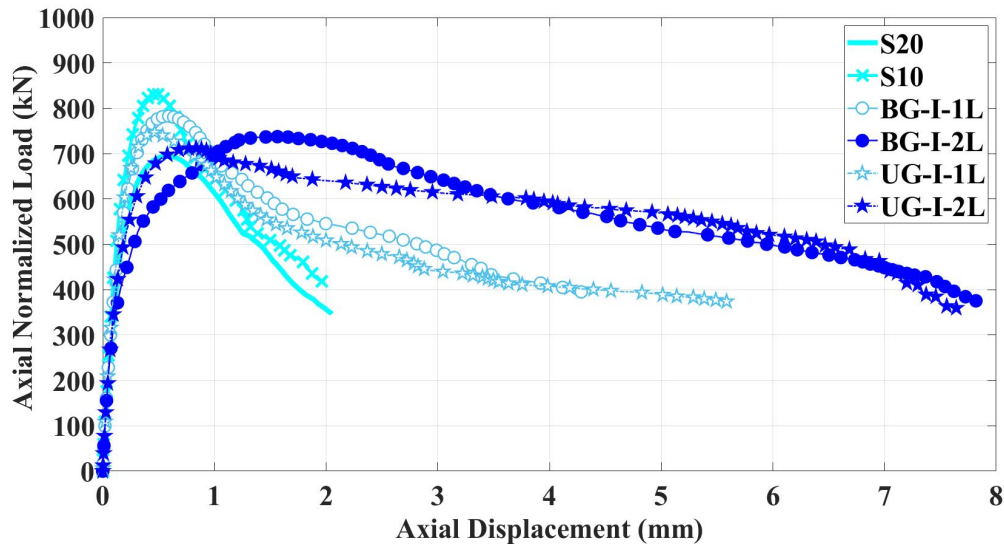


Figure 4.11: Load-displacement curves for internally confined specimens

#### 4.2.2.2 External confinement

The external confinement using any of the confinement materials included in the research provided overall confinement for the whole specimen contrary to the internal confinement, which is limited to the core area around the longitudinal steel reinforcement. All the externally confined specimens surpassed the axial load capacity and ductility of the control specimen S20.

Figure 4.12 shows the load-displacement curves of all specimens externally confined with biaxial geogrid, uniaxial geogrid, and bitumen textile sheets along with the tie specimens S20 (Control) and S10. Referring to Table 4.1 and Figure 4.7, specimens externally confined using one or two layers of uniaxial or biaxial geogrid reached higher loads than the internally geogrid confined specimens. The double layer external geogrid confined specimens, uniaxial and biaxial, had axial load capacities very similar to S10.

On the other hand, specimens externally confined with one and two layers of bitumen textile sheets scored on the average around 30% higher axial load capacity than S20 and around 10% more capacity than the double layered externally confined geogrid specimens. The higher axial load capacity of the bitumen textile sheets specimens could be related due to the sheet wrapping technique: whereas the flexible bitumen textile sheets had direct contact with the concrete column specimen, both the biaxial and uniaxial geogrid sheets required steel wires to closely wrap them around the concrete column specimens due to their rigidity. Thus the contact of the geogrid sheets with the confined concrete surface was not full and continuous as compared to the bitumen textile sheets. However, although the externally confined bitumen textile sheet specimens, single and double lay-

ered, had better load capacity than all the geogrid confined specimens, however this load superiority did not extend to the ductility indices whose values were on the average lower than all geogrid confined specimens internally and externally. This could be related to the flexibility of the bitumen sheets as compared to the rigid geogrid sheets which improved the post-ultimate load-displacement behavior after the lateral expansion of the concrete specimen made the contact with the rigid geogrid sheets more effective.

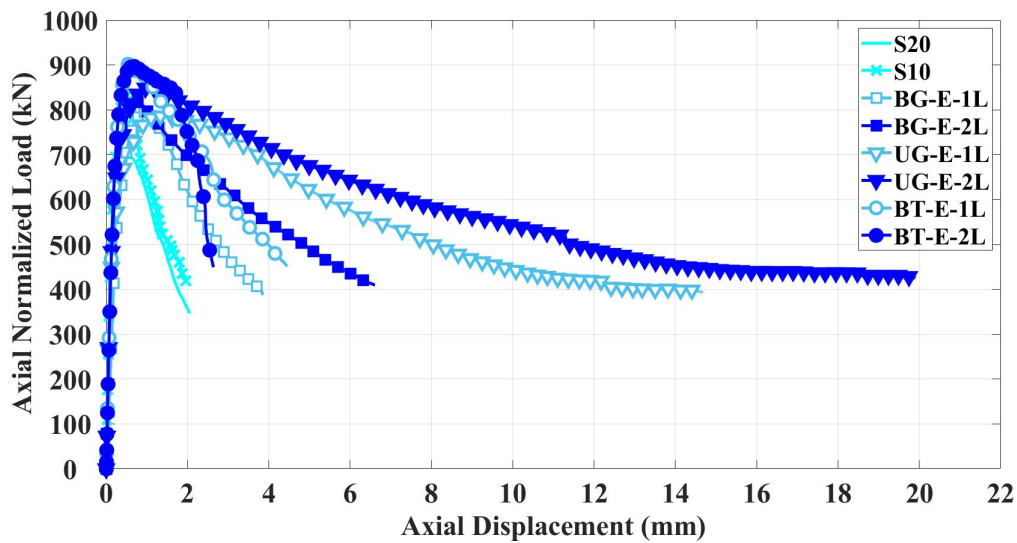


Figure 4.12: Load-displacement curves of geogrid and bitumen textile externally confined specimens along with specimens S20 (Control) and S10

#### 4.2.2.3 Internal versus external geogrid confinement

To show the difference between the load-displacement behaviors of internally and externally confined specimens using biaxial geogrids, reference is made to Figure 4.13, Table 4.1, and Figures 4.8 and 4.9. It could be seen that the two externally confined biaxial geogrid specimens, with one and two geogrid layers, had on the average 6% higher ultimate load than the internally confined ones. However, the energy dissipation and ductility indices of the externally confined biaxial geogrid specimens were on the average similar to the two internally confined biaxial geogrid specimens. These indices are higher than those of the best performing tie confined specimen S10.



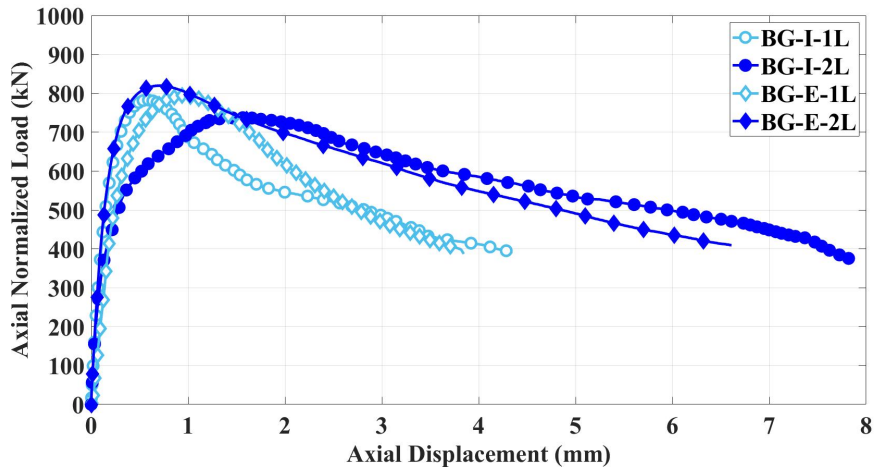


Figure 4.13: Load-displacement curves of internally and externally confined bi-axial geogrid Specimen, single and double layered

On the other hand, the difference between the load-displacement behaviors of internally and externally confined specimens using uniaxial geogrids is shown in Figure 4.14. Referring to Figure 4.14, Table 4.1, and Figures 4.8 and 4.9, the two externally confined uniaxial geogrid specimens, with one and two geogrid layers, had on the average 12% higher ultimate load than the internally confined ones. Both the internally and externally confined uniaxial geogrid specimens had higher displacement ductility index than all the specimens tested in the experimental program, with the externally confined ones having more than double the displacement and energy ductility indices than the internally confined ones.

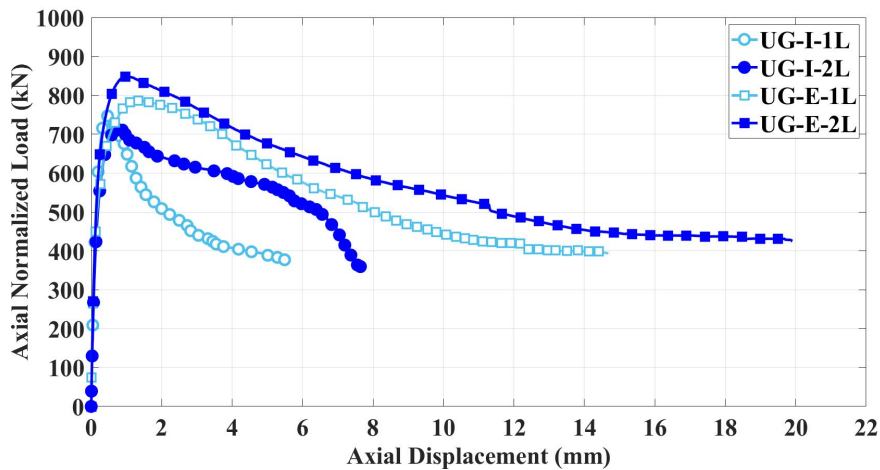


Figure 4.14: Load-displacement curves of internally and externally confined bi-axial geogrid Specimen, single and double layered

#### 4.2.2.4 External FRP versus external geogrid confinement

Figure 4.15 shows the load-displacement curves of the biaxial geogrid, uniaxial geogrid, and FRP externally confined specimens, one layered and double layered. Referring to Table 4.1 and Figure 4.7, the FRP confined specimens had the highest axial load capacity as compared to all other tested specimens. As compared to the best performing externally confined uniaxial geogrid double layer specimen UG-E-2L, the increase in axial load capacity was 67% for the single layer FRP specimen FRP-E-1L and 127% for the double layer FRP specimen FRP-E-2L. This could be attributed to the larger tensile strength of the FRP sheets as compared to the geogrid sheets. On the other hand, the load-displacement curves shown in Figure 4.15 and the displacement ductility indices displayed in Table 4.1 and Figure 4.8 clearly indicate that the externally confined uniaxial geogrid specimens, single and double layered, exhibited much higher displacements at failure as compared the biaxial geogrid and the FRP specimens which were similar. However, comparing fracture energy dissipation, values listed in Table 4.1 and shown in Figure 4.9 clearly indicate that the double layered FRP specimen had the highest k value (12.27), as compared to 2.05 and 3.63 for the single and double layered biaxial geogrid specimens, respectively, and as compared to 7.47 and 8.49 for the single and double layered uniaxial geogrid specimens, respectively.

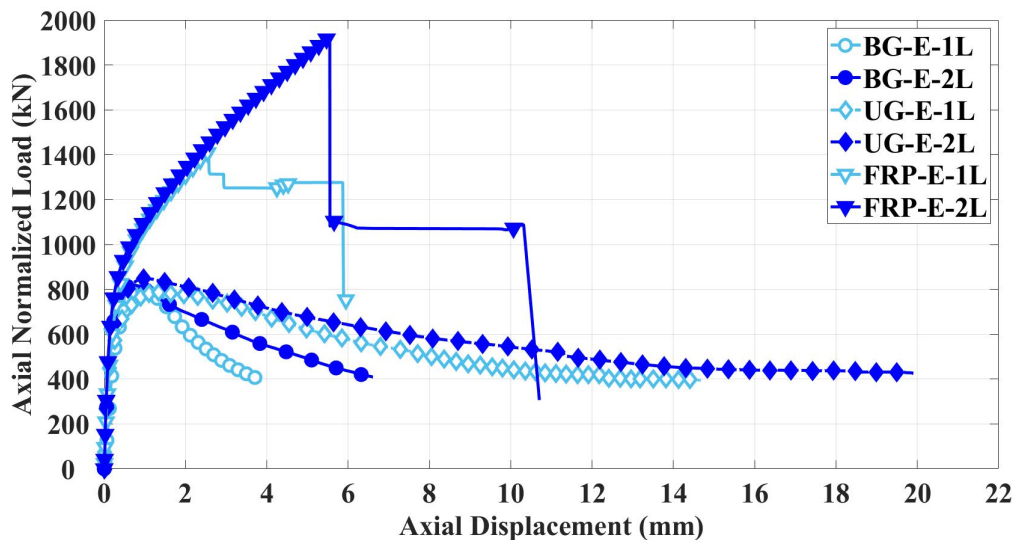


Figure 4.15: Load-displacement curves of geogrid and FRP Sheet externally confined specimens

### 4.3 Prediction of ultimate axial stresses

The existing analytical models for externally confined specimens, available in the literature, were developed for confining materials such as FRP which have constant thickness and fully cover the external surface of the confined concrete specimens. However, [Michael et al., 2005] developed an analytical model to verify and predict the experimental results of a study of CFRP grid confined cylindrical specimens. The intention of this part of the reported research was to modify the analytical model proposed by [Michael et al., 2005] to be applicable to the externally geogrid confined reinforced concrete column specimens tested in this research.

The study of [Michael et al., 2005] was designed to study the confinement effect of embedded CFRP grids, tied into a circular shape and cast into the concrete in a similar configuration to spiral ties, on the strength of 152x304 mm concrete cylinders. The CFRP grid used by Michael et al. was fabricated from carbon fibers embedded in an epoxy matrix (refer to Figure 19). The spacings of the CFRP grid strands were 45.7 and 40.6 mm in the longitudinal and transverse directions, respectively. The average tensile strength of the grid was approximately 695.5 MPa and the average tensile modulus was 64.5 GPa.

The model proposed by [Michael et al., 2005] for CFRP grid confined specimens was based on assuming that the confined concrete cylindrical section is in a triaxial stress state. According to [Mander et al., 1988], the maximum stress  $f'_{cc}$  for a cylindrical specimen is defined as:

$$f'_{cc} = f'_c + k_1 \cdot f_{ru} \quad (4.1)$$

Where  $k_1$  is the confinement effectiveness coefficient which is usually taken between 2.8 and 4.1 for concrete confined by steel. [Campione and Miraglia, 2003] found that the above values overestimate the value of  $k_1$  for concrete wrapped with FRP, and they recommended a value of 2 instead. Therefore, [Michael et al., 2005] used a value of 2 for  $k_1$  in their proposed model.  $f_{ru}$  is the confinement strength determined using Equation 4.2.

$$f_{ru} = \frac{2 \cdot t_{eq}}{d_g} \cdot f_{gu} \quad (4.2)$$

Where  $f_{gu}$  is the ultimate strength of the CFRP grid strands,  $d_g$  is the diameter of the CFRP grid tube, and  $t_{eq}$  is the equivalent CFRP grid thickness calculated by [Michael et al., 2005] using Equation 3.

$$t_{eq} = \frac{n_l \cdot n_{gs} \cdot b_g \cdot t_g}{h} \quad (4.3)$$

Where  $n_l$  is the number of the CFRP grid layers,  $n_{gs}$  is the number of grid strands,  $b_g$  is the width of the grid,  $t_g$  is the thickness of the grid, and  $h$  is the

height of the specimen. For columns, [Michael et al., 2005] simplified Equation 4.3 as follows:

$$t_{eq} = \frac{n_l \cdot b_g \cdot t_g}{s_g} \quad (4.4)$$

Where  $s_g$  is the grid strand spacing of the confining CFRP grid. Using the analytical model presented above, [Michael et al., 2005] found out that the average predicted peak stress of the CFRP grid confined specimens was 52 MPa as compared to the average experimental value of 52.9 MPa; i.e., the predicted value was 1.7% lower than the experimental value.

To apply the analytical model of [Michael et al., 2005] on the tested specimens, the ultimate confinement strength  $f_{gu}$  in MPa was determined by multiplying the ultimate tensile strength  $T_{ult}$ , given in kN/m in Tables 3-5 for the different confining materials, by 1000 N/kN and dividing the answer by the number of ribs in one meter  $n_{rm}$  multiplied by the area of one rib  $A_r$ ;  $A_r$  is equal to the width of the rib  $b_g$  multiplied by the rib thickness  $t_g$ .

$$f_{gu}(MPa) = \frac{T_{ult}}{n_{rm} \cdot A_r} \quad (4.5)$$

Results of the analytical model in comparison with the experimental test results of 6 externally confined specimens are listed in Table 9. The model over-predicts the experimental results by 15% for the biaxial geogrid specimens, by 11 to 12% for the uniaxial geogrid specimens, and by 5 to 10% for the bitumen textile specimens. Therefore, a reduction factor  $\theta$  equal to 0.8 was suggested to be applied to the maximum stress  $f'_{cc}$  given in Equation 4.1:

$$f'_{cc} = \theta(f'_c + k_l \cdot f_{ru}) \quad (4.6)$$

The reasoning behind this reduction factor is the reduced effectiveness of the confinement of geogrids as compared to the CFRP grid material. The geogrid sheets shown in Figures 1a and 1b have connecting joints (called junction for the biaxial geogrid and transverse rib for the uniaxial geogrid) which are thicker than the rib thickness. At the beginning of the loading history, the contact between the confined concrete and the geogrid sheets is at the junctions. As the loading progresses and the concrete expands laterally, more contact is registered between the concrete specimen and the geogrid. Model results using Equation 6 are shown in Table 10. The modified analytical model results are 6% less than the experimental results for the biaxial geogrid specimens, 2% to 3% greater than the experimental results for the uniaxial specimens, and 13% to 19% less than the experimental results for the bitumen textile specimens. Example of the calculation of  $f'_{cc}$  for specimen BG-E-1L using Equation 4.6, is given in the Appendix.

Table 4.2: Results of the analytical model without reduction factor

Equation	$f_{cc} = f_{co} + 2.f_{ru}$		
Confinement Type	$P_{test}$	$P_{model}$	$P_{test}/P_{model}$
BG-E-1L	17.55	20.72	0.85
BG-E-2L	18.12	21.44	0.85
UG-E-1L	17.39	22.10	0.79
UG-E-2L	18.76	24.20	0.78
BT-E-1L	19.95	20.98	0.95
BT-E-2L	19.84	21.96	0.90

Table 4.3: Results of the analytical model applying a reduction factor

Equation	$f_{cc} = \theta(f_{co} + 2.f_{ru})$		
Confinement Type	$P_{test}$	$P_{model}$	$P_{test}/P_{model}$
BG-E-1L	17.55	16.58	1.06
BG-E-2L	18.12	17.15	1.06
UG-E-1L	17.39	17.68	0.98
UG-E-2L	18.76	19.36	0.97
BT-E-1L	19.95	16.78	1.19
BT-E-2L	19.84	17.57	1.13

# Chapter 5

## Conclusion and Recommendations

### 5.1 Conclusion

The objective of the research study was to investigate the feasibility of using geogrid as external confinement for circular reinforced concrete columns. A total of 39 small-scale column specimens were tested under uniaxial compression. The main test variables were: transverse reinforcement spacing, confinement material (Geogrid, Bitumen coated E-glass textile, or CFRP), type of geogrid (uniaxial or biaxial), number of confinement layers (one or two), confinement location (internal or external). The experimental results were presented, analyzed, and compared to different analytical confinement models available in the literature. Based on the test results, the following conclusions can be drawn:

1. Under simulated monotonic loading, the use of geogrid confinement, internally and externally, can develop ductile behavior. External confinement with geogrids increases the deformability of columns much more than the closely spaced ties and internal geogrid confinement.
2. External confinement of the column specimens with one geogrid layer led to increase in the axial load capacity by an average of 14% as compared with the control specimen S20 with ties spaced at 20 cm. Using two layers of geogrid, the axial load capacity was approximately equal to that of the closely spaced tie specimen S10, with an increase of 20% as compared to the control specimen S20.
3. Internal confinement of the column specimens with one layer of geogrid led to increase by an average of 10% in the axial load capacity as compared with the control specimen S20. Using two layers of internal geogrid confinement led to slight reduction in the axial load capacity as compared to the single layer confinement mainly due to the reduction of the clear concrete cover.
4. External confinement of the column specimens by one layer of bitumen textile led to increase by an average of 10% in the axial load capacity as compared with

the closely spaced ties S10. Using two layers of bitumen textile did not have any significant effect on either axial load capacity or the ductility of the specimen.

5. FRP sheets had the best performance in the axial load capacity which increased by 104% and 178% using one and two layers, respectively. However, the brittle mode of failure of FRP confined specimens was reflected in their relatively very low displacement ductility index, much lower than all other specimens.

6.6. The analytical model proposed by [Michael et al., 2005] for CFRP grid internally confined specimens was modified to predict the ultimate capacity of the geogrid confined reinforced concrete specimens of this study.

7. Experimental test results were compared with the values predicted using different analytical models. For the scope covered in this research, the model of [Youssef et al., 2007] gave closer stress values to the experimental results than other models.

## 5.2 Recommendation

Future research is needed to further our understanding of the behavior of using geogrids as internal and external confinement techniques of reinforced concrete columns. This could include:

- 1- Applying geogrid confinement internally only between the ties.
- 2- Applying geogrid confinement externally without the epoxy layer.
- 3- Applying geogrid confinement externally in the form of strips rather than a full sheet.

# Appendix A

## Biaxial Geogrid Confinement Model Example

Confinement model – Example on Biaxial Geogrid Specimen 50 cm long –  
1 layer biaxial geogrid confinement Table 3.2 summarizes the properties of the  
biaxial geogrids used in this study.

Number of geogrid layers:  $n_l = 1$

Rib width:  $b_g = 2.2\text{mm}$

Rib thickness:  $t_g = 2.2\text{ mm}$

Area of rib:  $A_r = b_g \cdot t_g = 2.2 \cdot 2.2 = 4.84\text{ mm}^2$

Rib spacing;  $s_g = 33\text{ mm}$

Number of ribs per meter,  $n_{rm} = 30$

Height of specimen:  $h = 50\text{mm}$

Specimen diameter:  $D = 240\text{mm}$

Normalized unconfined concrete stress:  $f_{co} = 20\text{ MPa}$

Equivalent thickness of uniform membrane:

$$t_{eq} = \frac{n_l \cdot b_g \cdot t_g}{s_g} = \frac{1 \cdot 2.2 \cdot 2.2}{33} = 0.15\text{mm}$$

$$\text{Geogrid ultimate strength, } f_{gu} = T_{ult} * \frac{1000 \frac{N}{kN}}{n_{rm} \frac{rib}{m} * A_r \frac{mm^2}{rib}} = 40 * \frac{1000}{40 * 4.88} = 275.5\text{MPa}$$

$$\text{Confinement strength, } f_{ru} = \frac{2 \cdot t_g}{d_g} * f_{gu} = \frac{2 * 0.157}{240} * 275.5 = 0.36\text{ MPa}$$

$$\text{Peak stress, } f_{cc} = \theta(f_c + 2 \cdot f_{ru}) = 0.8 * (20 + 2 * 0.36) = 16.58\text{MPa}$$



# Bibliography

- [ACI-440.2R-08, 2002] ACI-440.2R-08 (2002). Guide for the design and construction of externally bonded frp systems for strengthening concrete structures. *Reported by ACI Committee*, 440(2002).
- [Al-Ayash et al., 2015] Al-Ayash, Z., Kahil, S., Karakashian, A., Mrad, M., Chehab, G., and Saad, G. (2015). Application of existing numerical models for prediction of geogrid confinement effectiveness of pcc columns. In *Proc., Geosynthetics Conf. Roseville, MN: Industrial Fabrics Association International*.
- [ASTM-C39, 2016] ASTM-C39 (2016). Standard test method for compressive strength of cylindrical concrete specimens.
- [ASTM-C617/C617M, 2012] ASTM-C617/C617M (2012). Standard practice for capping cylindrical concrete specimens.
- [ASTM-D6637/D6637M-15, 2021] ASTM-D6637/D6637M-15 (2021). Standard test method for determining tensile properties of geogrids by the single or multi-rib tensile method.
- [Bournas et al., 2007] Bournas, D. A., Lontou, P. V., Papanicolaou, C. G., and Triantafillou, T. C. (2007). Textile-reinforced mortar versus fiber-reinforced polymer confinement in reinforced concrete columns. *ACI Structural Journal*, 104(6):740.
- [Campione and Miraglia, 2003] Campione, G. and Miraglia, N. (2003). Strength and strain capacities of concrete compression members reinforced with frp. *Cement and Concrete Composites*, 25(1):31–41.
- [Chidambaram and Agarwal, 2014] Chidambaram, R. S. and Agarwal, P. (2014). The confining effect of geo-grid on the mechanical properties of concrete specimens with steel fiber under compression and flexure. *Construction and Building Materials*, 71:628–637.

- [Daou et al., 2020] Daou, A., Chehab, G., Saad, G., and Hamad, B. (2020). Experimental and numerical investigations of reinforced concrete columns confined internally with biaxial geogrids. *Construction and Building Materials*, 263:120115.
- [Daou, 2018] Daou, A. Y. (2018). An experimental and numerical assessment of the behavior of geogrid-reinforced concrete columns.
- [Das et al., 2010] Das, B., Penman, J., and Anderson, P. (2010). Use of geogrid in subgrade-ballast system of railroads subjected to cyclic loading for reducing maintenance. *California State University, Sacramento, USA*.
- [Das, 2016] Das, B. M. (2016). Use of geogrid in the construction of railroads. *Innovative Infrastructure Solutions*, 1(1):1–12.
- [Doğan and Arslan, 2016] Doğan, G. and Arslan, M. H. (2016). Failure modes of rc columns under loading. *International Journal of Scientific Engineering Research*.
- [El Meski and Chehab, 2014] El Meski, F. and Chehab, G. (2014). Flexural behavior of concrete beams reinforced with different types of geogrids. *Journal of materials in civil engineering*, 26(8):04014038.
- [Fajfar, 2018] Fajfar, P. (2018). Analysis in seismic provisions for buildings: past, present and future. In *European Conference on Earthquake Engineering Thessaloniki, Greece*, pages 1–49. Springer.
- [Ghafoori et al., 2016] Ghafoori, N., Sharbaf, M., et al. (2016). Use of geogrid for strengthening and reducing the roadway structural sections. Technical report, Nevada. Dept. of Transportation.
- [Ghalieh et al., 2017] Ghalieh, L., Awwad, E., Saad, G., Khatib, H., and Mab-sout, M. (2017). Concrete columns wrapped with hemp fiber reinforced polymer—an experimental study. *Procedia engineering*, 200:440–447.
- [Han et al., 2013] Han, X.-l., Ji, J., et al. (2013). Failure mode classification of reinforced concrete column using fisher method. *Journal of Central South University*, 20(10):2863–2869.
- [Harajli et al., 2010] Harajli, M., ElKhatib, H., and San-Jose, J. T. (2010). Static and cyclic out-of-plane response of masonry walls strengthened using textile-mortar system. *Journal of materials in civil engineering*, 22(11):1171–1180.
- [Hernandez et al., 2015] Hernandez, O., El Naggar, H., and Bischoff, P. H. (2015). Soil-structure interaction of steel fiber reinforced concrete slab strips on a geogrid reinforced subgrade. *Geotechnical and Geological Engineering*, 33(3):727–738.

- [Ilki et al., 2008] Ilki, A., Peker, O., Karamuk, E., Demir, C., and Kumbasar, N. (2008). Frp retrofit of low and medium strength circular and rectangular reinforced concrete columns. *Journal of Materials in Civil Engineering*, 20(2):169–188.
- [Itani et al., 2016] Itani, H., Saad, G., and Chehab, G. (2016). The use of geogrid reinforcement for enhancing the performance of concrete overlays: An experimental and numerical assessment. *Construction and Building Materials*, 124:826–837.
- [Kal et al., 2009] Kal, K.-W., Lee, D.-H., Bang, Y.-S., Cho, H.-C., Kang, J.-O., and Kim, K.-S. (2009). The effectiveness of steel fibers as shear reinforcement. In *Proceedings of the Korea Concrete Institute Conference*, pages 59–60. Korea Concrete Institute.
- [Lam and Teng, 2003] Lam, L. and Teng, J. G. (2003). Design-oriented stress-strain model for frp-confined concrete. *Construction and building materials*, 17(6-7):471–489.
- [Mander et al., 1988] Mander, J. B., Priestley, M. J., and Park, R. (1988). Theoretical stress-strain model for confined concrete. *Journal of structural engineering*, 114(8):1804–1826.
- [Maxwell, 2005] Maxwell, S. (2005). *Effectiveness of geosynthetics in stabilizing soft subgrades*. Wisconsin Highway Research Program.
- [Michael et al., 2005] Michael, A., Hamilton III, H., and Ansley, M. (2005). Concrete confinement using carbon fiber reinforced polymer grid. *Special Publication*, 230:991–1010.
- [Mirmiran et al., 1998] Mirmiran, A., Shahawy, M., Samaan, M., Echary, H. E., Mastrapa, J. C., and Pico, O. (1998). Effect of column parameters on frp-confined concrete. *Journal of Composites for construction*, 2(4):175–185.
- [Palmeira et al., 2008] Palmeira, E. M., Tatsuoka, F., Bathurst, R. J., Stevenson, P. E., and Zornberg, J. G. (2008). Advances in geosynthetics materials and applications for soil reinforcement and environmental protection works. *Electronic Journal of Geotechnical Engineering*, 13:1–38.
- [Parvin and Wang, 2001] Parvin, A. and Wang, W. (2001). Behavior of frp jacketed concrete columns under eccentric loading. *Journal of Composites for construction*, 5(3):146–152.
- [Pessiki et al., 2001] Pessiki, S., Harries, K. A., Kestner, J. T., Sause, R., and Ricles, J. M. (2001). Axial behavior of reinforced concrete columns confined with frp jackets. *Journal of composites for Construction*, 5(4):237–245.

- [Sadeghian and Fam, 2015] Sadeghian, P. and Fam, A. (2015). Strengthening slender reinforced concrete columns using high-modulus bonded longitudinal reinforcement for buckling control. *Journal of structural Engineering*, 141(4):04014127.
- [Sivakamasundari et al., 2017] Sivakamasundari, S., Daniel, A. J., and Kumar, A. (2017). Study on flexural behavior of steel fiber rc beams confined with biaxial geo-grid. *Procedia engineering*, 173:1431–1438.
- [Spoelstra and Monti, 1999] Spoelstra, M. R. and Monti, G. (1999). Frp-confined concrete model. *Journal of composites for construction*, 3(3):143–150.
- [Tang et al., 2008] Tang, X., Chehab, G., and Kim, S. (2008). Laboratory study of geogrid reinforcement in portland cement concrete. In *Proceedings of the 6th RILEM International Conference on Cracking in Pavements*, pages 769–778.
- [Wu et al., 2006] Wu, Y.-F., Liu, T., and Oehlers, D. J. (2006). Fundamental principles that govern retrofitting of reinforced concrete columns by steel and frp jacketing. *Advances in Structural Engineering*, 9(4):507–533.
- [Youssef et al., 2007] Youssef, M. N., Feng, M. Q., and Mosallam, A. S. (2007). Stress–strain model for concrete confined by frp composites. *Composites Part B: Engineering*, 38(5-6):614–628.